

Removing numerical dispersion from linear evolution equations

Jens Wittsten, Erik F. M. Koene, Fredrik Andersson,
and Johan O. A. Robertsson

ABSTRACT. In this paper we describe a method for removing the numerical errors in the modeling of linear evolution equations that are caused by approximating the time derivative by a finite difference operator. We prove that the method results in a solution with correct evolution throughout the entire lifespan. We demonstrate the method on a model equation as well as on the simulation of elastic and viscoelastic wave propagation.

1. INTRODUCTION

The difference between a continuous differential equation and its discretized counterpart is a source of numerical artifacts. Generally, the discretized system differs from the intended system in its dispersive and dissipative properties, so errors in the computation are referred to as *numerical dispersion* and *numerical dissipation* [1]. Here dispersion refers to a process in which energy separates into its component frequencies as the solution evolves, while dissipation refers to damping of energy during the evolution. Numerical dispersion thus refers to phase errors, while numerical dissipation refers to amplitude errors. The combined effect of the two numerical errors is sometimes described as *numerical diffusion*, and their effect as a function of direction as *numerical anisotropy*.

Numerical diffusion errors are typically studied through the local truncation error, i.e., the consistency between the discrete and continuous equation in terms of the discrete step size. If the method is stable, the Lax equivalence theorem [14] implies that the discretized equation converges to its continuous counterpart. As a consequence, the majority of the numerical methods for differential equations are designed with the intent of minimizing the local truncation error, with the expectation that the global error will then also be small. Examples are high-order accurate derivative schemes [10, 7] and high-order accurate integration schemes such as Runge-Kutta or ADER (Arbitrary high order schemes using DERivatives) [9, 22, 8, 15]. The high-order techniques typically lead to more accurate results compared to low-order methods, but come with a trade-off in increased computational cost.

In this paper we shall analyze numerical errors not through the local error but by comparing numerical solutions to true solutions. By doing so we are able to demonstrate that linear evolution equations, solved with finite difference approximations, contain a numerical dispersion error that can be fully eliminated through usage of pre-computation and post-computation filters. This is true even for simple second-order finite difference approximations. The filters are known as the *forward time dispersion transform* and *inverse time dispersion transform*, respectively (see

Definition 2.2). Heuristically, applying the forward time dispersion transform as a pre-filter amounts to artificially injecting dispersion (caused by a finite difference approximation of the time derivative) equally to all terms of the finite difference equation. After having solved the obtained equation, numerical dispersion is then removed from the computed solution by applying the inverse time dispersion transform as a post-filter.

Such a method has previously been proposed for acoustic and elastic wave simulations in the geophysical literature in order to achieve near-spectral temporal accuracy using only standard second-order accurate time integration schemes [21, 24, 13]. Section 2 of this paper generalizes the method to a large class of linear evolution equations and proves that the proposed pre- and post-filtering yields a numerical solution that correctly models the desired evolution for any length of time (Theorem 2.7).

Section 3 demonstrates the theoretic results by conducting numerical tests on a model equation where the solution obtained by the proposed method compares to the analytic solution with double precision accuracy (see Figure 2). In Section 4 the results are also demonstrated for viscoelastic wave simulation, to show that the method can deal even with dissipative wave physics. The simulations show that the filtering procedure has the potential to overcome the typical trade-off in accuracy-vs-cost as the filters are cheap to apply, while still yielding highly accurate solutions.

Our findings are summarized in Section 5, and the paper is then concluded with three appendices. In Appendix A we have gathered results of tangential or supplementary nature referenced in the main text. In Appendix B one can find the implementation of the finite difference scheme used in the viscoelastic wave simulations. Finally, in Appendix C we provide codes for implementing the dispersion transforms in MATLAB.

2. NUMERICAL DISPERSION IN EVOLUTION EQUATIONS

Let $X \subset \mathbb{R}^d$ and $u = (u_1, \dots, u_K)$ be a vector valued function of $(t, x) \in \mathbb{R} \times X$. Introduce the $K \times K$ system of differential operators

$$\mathcal{P}_i u(t, x) = \partial_t^{n_i} u_i(t, x) + \sum_{j=0}^{n_i-1} \sum_{k=1}^K \partial_t^j L_{ijk} u_k(t, x), \quad 1 \leq i \leq K,$$

where $\partial_t^j u_k(t, x) = \partial^j u_k(t, x) / \partial t^j$ and the L_{ijk} are linear spatial operators depending on $x \in X$ but independent of time t so that ∂_t and L_{ijk} commute. Consider the initial value problem in $[t_0, \infty) \times X$ given by

$$(2.1) \quad \mathcal{P}_i u(t, x) = f_i(t, x), \quad 1 \leq i \leq K,$$

$$(2.2) \quad \partial_t^j u_i(t_0, x) = \phi_{ij}(x), \quad 1 \leq j \leq n_i - 1.$$

Since the system is translation invariant in t we may without loss of generality assume that $t_0 = 0$ below. We will assume that the problem is well posed and that, depending on the spatial operators L_{ijk} , appropriate spatial conditions are imposed to ensure a unique solution. For an extensive background on partial differential equations we refer to Hörmander [11] and Evans [5].

When solving (2.1)–(2.2) by means of finite difference (FD) methods, numerical dispersion errors inevitably occur as a result of approximating the time derivatives

with finite differences. The purpose of this paper is to establish a method by which to alter the chosen FD system and capture the correct time evolution of the solution u to (2.1)–(2.2). We will only be concerned with FD schemes which are numerically stable and depend continuously on the initial data. A comprehensive treatment of finite difference methods can be found in LeVeque [15].

In this work, the exact structure of the spatial operators is not essential. However, for simplicity we will assume that the f_i are integrable with respect to t , and that each L_{ijk} as well as the source terms f_i and initial data ϕ_{ij} are regular enough that (2.1)–(2.2) admits a strong solution u_i , integrable with respect to t , such that for each $1 \leq i \leq K$

$$(2.3) \quad t \mapsto \sup_{x \in X} |u_i(t, x)| \in H^{n_i}((-\infty, \infty)).$$

Here, $H^s = W^{s,2}$ is the usual L^2 Sobolev space of order s . (Obviously, by considering weak solutions and more precisely defined spatial operators L_{ijk} these regularity assumptions could be relaxed or refined, but that is not a direction we will pursue.) In particular, the partial Fourier transforms $\hat{u}_i(\omega, x)$ and $\hat{f}_i(\omega, x)$ are then well defined and locally integrable, where

$$\hat{u}_i(\omega, x) = \mathcal{F}(u_i(\cdot, x))(\omega) = \int_{-\infty}^{\infty} e^{-2\pi i t \omega} u_i(t, x) dt.$$

Remark. Realizations of the Cauchy problem (2.1)–(2.2) can for example be found in initial value problems for:

- (1) Ordinary differential equations with constant coefficients.
- (2) Heat equations, linear parabolic equations.
- (3) Wave equations, linearly damped wave equations, Maxwell's equations, linear elasticity.
- (4) Visco-acoustic and viscoelastic equations solved via memory variables (see §4.1).
- (5) Strictly hyperbolic pseudodifferential equations, Tricomi equations.

2.1. Finite difference system. Introduce the FD operators

$$P_i v(t, x) = D^{n_i} v_i(t, x) + \sum_{j=0}^{n_i-1} \sum_{k=1}^K D^j L_{ijk} v_k(t, x), \quad 1 \leq i \leq K,$$

corresponding to the partial differential operators \mathcal{P}_i discussed above. Here,

$$(2.4) \quad D^j v_i(t, x) = \sum_n c_{j,n} v_i(t + n\Delta t, x),$$

where n usually ranges over the set of integers or half-integers, and the coefficients $c_{j,n}$ are chosen so that D^j becomes an approximation of the j th order time derivative. As the notation indicates, we assume that

$$D^j = \underbrace{D \circ \dots \circ D}_j,$$

which can be translated into a condition for the coefficients $c_{j,n}$. For example, $D^2 = DD$ precisely when $c_{2,n} = \sum_k c_{1,k} c_{1,n-k}$. For the majority of the paper we also assume that the same scheme D is used as a basis for D^j in each of the K operators P_i . The case of non-matching finite difference schemes is discussed briefly on page 8 below and again in §A.3 in the appendix.

Taking a partial Fourier transform of (2.4) we observe that

$$(2.5) \quad \int_{-\infty}^{\infty} e^{-2\pi i t \omega} D^j v_i(t, x) dt = \left(\sum_n c_{1,n} e^{2\pi i \omega \Delta t n} \right)^j \widehat{v}_i(\omega, x).$$

In view of this identity and the fact that

$$\mathcal{F} \left(\partial_t^j u_i(\cdot, x) \right) (\omega) = (2\pi i \omega)^j \widehat{u}_i(\omega, x),$$

we define a *phase shift function* q as

$$(2.6) \quad q(\omega) = \frac{1}{2\pi i} \sum_n c_{1,n} e^{2\pi i n \omega \Delta t}$$

so that

$$\mathcal{F} \left(D^j v_i(\cdot, x) \right) (\omega) = (2\pi i q(\omega))^j \widehat{v}_i(\omega, x).$$

We will assume that $c_{1,n}$ is chosen in such a way that $q(\omega)$ is real-valued and invertible for $\omega \in \Omega$ for some subset $\Omega = \Omega(\Delta t) \subset \mathbb{R}$. For a comment on the case when q is not real-valued (which happens e.g., in the case of a forward Euler scheme), see the remark on page 7. Note also that with respect to the normalized variable $\omega \Delta t$, the right-hand side of (2.6) is invertible for all $\omega \Delta t$ belonging to some fixed, Δt -independent set. In fact, under the natural assumption that $c_{1,n} \Delta t$ is independent of Δt , it follows that

$$(2.7) \quad q_0(\eta) = q(\eta/\Delta t) \Delta t = \frac{1}{2\pi i} \sum_n (c_{1,n} \Delta t) e^{2\pi i n \eta}$$

is a trigonometric polynomial independent of Δt .

Example 2.1. Let D be given by (2.4) for $j = 1$, where the index n ranges over the integers, and choose coefficients $c_{1,\pm 1} = \pm 1/(2\Delta t)$ and $c_{1,n} = 0$ for all other values of n . Then D is the central difference operator

$$Dv(t) = \frac{v(t + \Delta t) - v(t - \Delta t)}{2\Delta t},$$

and $q(\omega) = \sin(2\pi \omega \Delta t)/2\pi \Delta t$. It follows that q is invertible for $\omega \in \Omega$ where $\Omega = [-\frac{1}{4\Delta t}, \frac{1}{4\Delta t}]$. In other words, q is invertible when the normalized variable $\omega \Delta t$ satisfies $|\omega \Delta t| \leq 1/4$. Moreover, $q_0(\eta) = \sin(2\pi \eta)/2\pi$.

2.2. Time dispersion transforms. Let $\mathbf{1}_\Omega$ denote the characteristic function of a set Ω , so that $\mathbf{1}_\Omega(\omega) = 1$ if $\omega \in \Omega$ and $\mathbf{1}_\Omega(\omega) = 0$ if $\omega \notin \Omega$. Based on the previous discussion we will henceforth assume that the function q introduced above is restricted to the largest subset $\Omega = \Omega(\Delta t)$ of its domain of definition, containing the origin if possible, where $q : \Omega \rightarrow q(\Omega)$ is invertible. The inverse q^{-1} is assumed to be defined on $q(\Omega)$.

Definition 2.2. Let $f_i(t, x)$ be a function integrable in t . Given a finite difference operator D , let q be the corresponding phase shift function in (2.6). Define the *forward time dispersion transform* (FTDT) of $f_i(t, x)$ as

$$(2.8) \quad \mathcal{T}(f_i)(t, x) = \int_{\Omega} e^{2\pi i t \omega} \widehat{f}_i(q(\omega), x) d\omega.$$

Define the *inverse time dispersion transform* (ITDT) of $f_i(t, x)$ by

$$(2.9) \quad \mathcal{I}(f_i)(t, x) = \int_{q(\Omega)} e^{2\pi i t \omega} \widehat{f}_i(q^{-1}(\omega), x) d\omega.$$

The definition extends in the natural way to distributions with well-defined Fourier transforms which are integrable on Ω . For example, the Dirac measure $\delta(t)$ has Fourier transform $\widehat{\delta}(\omega) \equiv 1$, so the FDTD of $\delta(t)$ is

$$\mathcal{T}(\delta)(t) = \int_{\Omega} e^{2\pi i t \omega} d\omega = \mathcal{F}^{-1}(\mathbf{1}_{\Omega})(t).$$

Example 2.3. Let $q(\omega) = \sin(2\pi\omega\Delta t)/2\pi\Delta t$ for $\omega \in [-\frac{1}{4\Delta t}, \frac{1}{4\Delta t}]$, so that q is the phase shift function corresponding to the finite difference operator in Example 2.1. Then

$$\mathcal{T}(\delta)(t) = \frac{1}{2\Delta t} \text{sinc}(\pi t/2\Delta t),$$

where $\text{sinc}(t) = \sin(t)/t$ is the sinc function.

For future purposes we record the fact that

$$(2.10) \quad \mathcal{I}(f_i)(t, x) = \int_{\Omega} e^{2\pi i t q(\omega)} \widehat{f}_i(\omega, x) q'(\omega) d\omega,$$

which follows by a straightforward change of variable. Similarly, we also have

$$(2.11) \quad \mathcal{T}(f_i)(t, x) = \int_{q(\Omega)} e^{2\pi i t q^{-1}(\omega)} \widehat{f}_i(\omega, x) \frac{1}{q'(q^{-1}(\omega))} d\omega.$$

Finally, note that

$$\mathcal{T}(f_i)(t, x) = \mathcal{F}^{-1} \left[\mathbf{1}_{\Omega}(\cdot) \widehat{f}_i(q(\cdot), x) \right](t),$$

which together with a straightforward calculation shows that

$$(2.12) \quad \mathcal{I}(\mathcal{T}(f_i))(t, x) = \int_{q(\Omega)} e^{2\pi i t \omega} \widehat{f}_i(\omega, x) d\omega.$$

In other words, $\mathcal{I}(\mathcal{T}(f_i))$ does not equal f_i , but the bandlimited version of f_i with frequency support contained in the range of q . However, in the context of implementation this is not a severe limitation of the transforms, since using an optimized algorithm such as the fast Fourier transform (FFT) in practice also imposes a limitation on the Fourier support. Nevertheless, the effect of (2.12) is analyzed in depth in what follows, in particular in Section 3.

Example 2.4. Consider again the case when $q(\omega) = \sin(2\pi\omega\Delta t)/2\pi\Delta t$ for $\omega \in [-\frac{1}{4\Delta t}, \frac{1}{4\Delta t}]$. Let f be a bandlimited function so that $f(t) = \mathcal{F}^{-1}(\mathbf{1}_{[-B, B]} \widehat{f})(t)$ for some minimal number B (the bandwidth). By the Nyquist-Shannon sampling theorem, the sampling rate necessary to accurately represent f is $f_s > 2B$. However, in order to utilize the entire frequency content of f when computing the forward dispersion transform $\mathcal{T}(f)$, the sampling rate has to be doubled since $[-B, B] \subset \Omega$ if and only if $B < \frac{1}{4\Delta t}$, i.e., $f_s = 1/\Delta t > 4B$. Furthermore, the sampling rate has to be effectively tripled in order for $\mathcal{I}(\mathcal{T}(f))$ to equal f , since $[-B, B] \subset q(\Omega)$ if and only if

$$B < q(1/4\Delta t) = \frac{1}{2\pi\Delta t},$$

i.e., $f_s = 1/\Delta t > 2B\pi$. These drawbacks can sometimes be removed, respectively improved, by using a staggered grid provided that the original equation (2.1) permits such leapfrog discretization schemes. See Section 4 and Appendix B for such an example.

We shall now examine the applications of Definition 2.2 for evolution equation modeling. We begin by showing that utilizing the FTDT to correct for numerical dispersion in the finite difference scheme guarantees that the solution evolves correctly for all time. This is made precise in the following theorem.

Theorem 2.5. *Let $u = (u_1, \dots, u_K)$ be a solution to the evolution equation (2.1). Set $g_i = \mathcal{T}(f_i)$ and $v_i = \mathcal{T}(u_i)$. Then $v = (v_1, \dots, v_K)$ solves the finite difference system*

$$(2.13) \quad \mathbf{P}_i v(t, x) = g_i(t, x), \quad 1 \leq i \leq K,$$

for each value of t .

Proof. First note that applying the Fourier transform to (2.1) and evaluating at $q(\omega)$ gives

$$(2.14) \quad (2\pi i q(\omega))^{n_i} \widehat{u}_i(q(\omega), x) + \sum_{j=0}^{n_i-1} \sum_{k=1}^K (2\pi i q(\omega))^j L_{ijk} \widehat{u}_k(q(\omega), x) = \widehat{f}_i(q(\omega), x).$$

Next, using the definition of \mathbf{P}_i together with (2.5)–(2.6) we get

$$\mathbf{P}_i v_i(t, x) = \int_{-\infty}^{\infty} \left[(2\pi i q(\omega))^{n_i} \widehat{v}_i(\omega, x) + \sum_{j=0}^{n_i-1} \sum_{k=1}^K (2\pi i q(\omega))^j L_{ijk} \widehat{v}_k(\omega, x) \right] e^{2\pi i t \omega} d\omega$$

by the Fourier inversion formula. Now substitute $\widehat{v}_i(\omega, x) = \mathbf{1}_{\Omega}(\omega) \widehat{u}_i(q(\omega), x)$ and use (2.14) to obtain

$$\mathbf{P}_i v_i(t, x) = \int_{\Omega} \widehat{f}_i(q(\omega), x) e^{2\pi i t \omega} d\omega.$$

By construction, the right-hand side equals $g_i(t, x)$, and the proof is complete. \square

We conclude this subsection with a few general remarks.

Fourier integral operators. Close inspection of (2.10) and (2.11) using the normalized phase shift function $q_0(\eta)$ defined in (2.7) shows that the dispersion transforms \mathcal{I} and \mathcal{T} can be formally interpreted as *Fourier integral operators* depending on a small semiclassical parameter $h = \Delta t$ (see Appendix A.1). As such, they are associated with a canonical map χ and its inverse χ^{-1} acting on phase space via

$$(2.15) \quad \chi : (t q'_0(\eta), \eta) \mapsto (t, q_0(\eta)).$$

The physical meaning of this is well understood in terms of dynamics of wave packets [6]. We provide a detailed presentation in §A.1.1, briefly summarized as follows: let (t_0, η_0) be a point in phase space and consider a *Gaussian wave packet* defined by

$$\varphi_{(t_0, \eta_0)}(t) = (2/\Delta t)^{\frac{1}{4}} e^{2\pi i(t-t_0)\eta_0/\Delta t} e^{-\pi(t-t_0)^2/\Delta t}.$$

When $t \neq t_0$ we have $\varphi_{(t_0, \eta_0)}(t) = O(\Delta t^\infty)$ as $\Delta t \rightarrow 0$, where $O(\Delta t^\infty)$ means $O(\Delta t^N)$ for all $N > 0$. Similarly, the semiclassical (i.e., scaled) Fourier transform

$$(2.16) \quad \begin{aligned} \mathcal{F}_{\Delta t}(\varphi_{(t_0, \eta_0)})(\eta) &= (\Delta t)^{-\frac{1}{2}} \mathcal{F}(\varphi_{(t_0, \eta_0)})(\eta/\Delta t) \\ &= (2/\Delta t)^{\frac{1}{4}} e^{-2\pi i t_0 \eta/\Delta t} e^{-\pi(\eta-\eta_0)^2/\Delta t} \end{aligned}$$

is $O(\Delta t^\infty)$ as $\Delta t \rightarrow 0$ if $\eta \neq \eta_0$. Such a function is said to be *microlocally small* outside $\{(t_0, \eta_0)\}$. By Proposition A.2, the ITDT of $\varphi_{(t_0, \eta_0)}$ is microlocally small outside

$$\{\chi(t_0, \eta_0)\} = \{(t_0/q'_0(\eta_0), q_0(\eta_0))\}$$

and the FDTD of $\varphi_{(t_0, \eta_0)}$ is microlocally small outside

$$\{\chi^{-1}(t_0, \eta_0)\} = \{(t_0 q'_0(q_0^{-1}(\eta_0)), q_0^{-1}(\eta_0))\}.$$

Thus in this sense, as $\Delta t \rightarrow 0$, the ITDT of $\varphi_{(t_0, \eta_0)}$ behaves like the wave packet $\varphi_{\chi(t_0, \eta_0)}$ and the FDTD of $\varphi_{(t_0, \eta_0)}$ behaves like the wave packet $\varphi_{\chi^{-1}(t_0, \eta_0)}$. This phenomenon is illustrated in Figure 1.

We also mention that by using arguments similar to those in the proof of Theorem 2.5, it is straightforward to check that $\mathcal{T}\mathcal{P}_i = \mathcal{P}_i\mathcal{T}$. Viewing the dispersion transforms as Fourier integral operators, the proof of Theorem 2.5 would then proceed by simply noting that, by assumption, $v_i = \mathcal{T}u_i$ and $g_i = \mathcal{T}f_i$, so

$$\mathcal{P}_i v_i = \mathcal{P}_i \mathcal{T}u_i = \mathcal{T}\mathcal{P}_i u_i = \mathcal{T}f_i = g_i.$$

In the sequel we shall continue to prefer elementary proofs using explicit formulas instead of relying on the framework of microlocal analysis. However, this interpretation does succinctly highlight the obstruction caused by allowing time-dependent coefficients in (2.1), see the discussion in Appendix A.1.

Initial conditions. These are not mentioned in Theorem 2.5. In fact, since the initial conditions are time-independent, they cannot be modified using the time dispersion transform so the natural choice is to impose the same initial conditions for (2.13) as for (2.1); this is also motivated by the fact that at time $t = 0$, dispersion should not yet have started to affect the numerical solution. However, suppose that u_i is the solution to (2.1) with initial conditions (2.2), and let v_i be the solution to (2.13) with the same initial conditions. Due to the non-local nature of the dispersion transforms, this introduces an approximation error between $\mathcal{T}(u_i)$ and v_i , described by the difference between $\partial_t^j \mathcal{T}(u_i)|_{t=0}$ and ϕ_{ij} in (2.2). On the other hand, according to Lemma A.3 this error is small and controlled by the time-step size Δt (see §A.2 for precise statements). Since $\mathcal{T}(u_i)$ and v_i have the same evolution in time according to Theorem 2.5, $\mathcal{T}(u_i)$ will thus continue to stay close to v_i for all time. The introduction of this error is also mitigated by the fact that when both dispersion transforms are used together in a modeling scenario as pre- and post-filters, then a reverse error is introduced during the post-filtering process. This is given credence by the numerical results in Sections 3 and 4. In view hereof we will from now on always assume that unless stated to the contrary, initial conditions are given by (2.2), with left-hand side discretized in the case of finite difference systems.

Backward and forward type schemes. In this case, the phase shift function q will not be real-valued in general. Still, under certain conditions one can define a version of the FDTD and ITDT, although this requires sufficiently fast (exponential) decay of the solutions $t \mapsto u_i(t)$ for the definitions above to make sense. However, when convergence is not an issue (such as when working with finite sums approximating the Fourier transform), or if u_i decays fast enough for the integral

$$\int_{-\infty}^{\infty} e^{-2\pi i t q(\omega)} u_i(t, x) dt$$

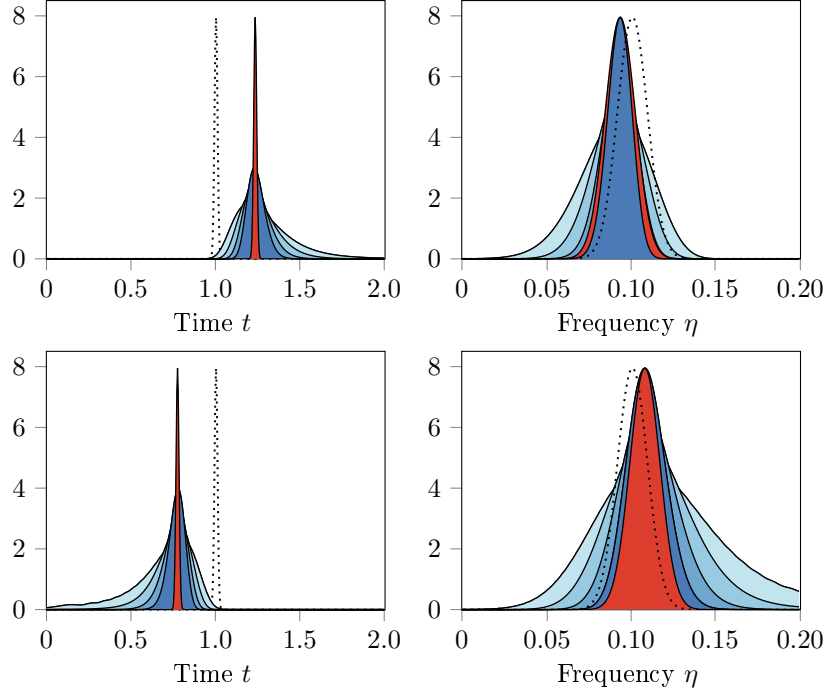


FIGURE 1. The inverse (top) and forward (bottom) dispersion transforms of a wave packet $\varphi_{(t_0, \eta_0)}$ in the time domain (left) together with their scaled Fourier transforms (right, cf. (2.16)), represented in blue by their corresponding modulus. Here $t_0 = 1$ and $\eta_0 = 0.1$, the normalized phase shift function is $q_0(\eta) = \sin(2\pi\eta)/2\pi$, and the ITDT and FTDT of $\varphi_{(t_0, \eta_0)}$ are computed for Δt ranging from 4 ms (light) to 0.5 ms (dark). In addition, $\varphi_{(t_0, \eta_0)}$ (dotted) as well as the wave packets microlocalized at $\chi(t_0, \eta_0)$ (red, top) and at $\chi^{-1}(t_0, \eta_0)$ (red, bottom) together with their scaled Fourier transforms are shown for $\Delta t = 0.5$ ms as reference.

to converge for all $\omega \in \Omega$, then Theorem 2.5 immediately generalizes to cover this situation. This happens, e.g., if $u_i(t, x) \equiv 0$ for $t < 0$, $|u_i(t, x)| \leq Ce^{-2\pi\alpha t}$ for some constants C and α , and $\text{Im } q(\omega) < \alpha$ for $\omega \in \Omega$. In particular, $v_i(t, x) = \mathcal{T}(u_i(\cdot, x))(t)$ is well defined. We leave it to the interested reader to fill in the details.

Nonmatching finite difference schemes. Due to the coupled nature of (2.1) it was essential in the proof of Theorem 2.5 that the same FD approximation of the time derivative was used for all involved operators \mathcal{P}_i . As soon as this is not the case, the result ceases to hold without appropriate modifications. For comparison, one such example of nonmatching finite difference schemes is provided in §A.3.

2.3. Discrete transforms. Theorem 2.5 shows how to use the FTDT to compensate for numerical dispersion when passing from a continuous equation to a discretized equation. We shall now investigate the converse situation utilizing the ITDT instead. Since we want to apply the ITDT to a solution of an FD equation

modified using the FDTD, we must first introduce suitable discrete versions of the transforms. In the process, we will obtain a methodology for correctly simulating the solution to an evolution equation of type (2.1).

We will demonstrate how to simulate the solution for $0 \leq t \leq T$, where $T > 0$ is the desired lifespan. Discretizing the equations and correcting for time dispersion leads us to solve the difference system (2.13). Suppose therefore that v_i is a computed solution to (2.13), with known values $v_i(t_n, x)$ at times $t_n = n\Delta t$, $0 \leq n < T/\Delta t$. (We describe below how to compute the right-hand side of (2.13) using discrete sums.) We assume that $T/\Delta t = N$ for some integer N , so that

$$\Delta t = T/N,$$

and denote by S the set of sampling points

$$S = \{n\Delta t : 0 \leq n < N\}.$$

We begin with a general discussion and let $f(t)$ be a function of $t \in [0, T]$ with known values at the points in S . Let $\omega_m \in \Omega$ and introduce

$$a_m(f) = \Delta t \sum_{n=0}^{N-1} f(n\Delta t) e^{-2\pi i n \Delta t \omega_m}.$$

This is a Riemann sum of the integral $\int_0^T f(t) e^{-2\pi i t \omega_m} dt$ and as such an approximation of $\hat{f}(\omega_m)$ provided f vanishes outside $[0, T]$. Inspecting the definition (2.10) of $\mathcal{I}(f)$ we then choose a partition of Ω and define a function of the continuous variable $t \in [0, T]$ via

$$(2.17) \quad \mathcal{I}_{\text{disc}}(f)(t) = \Delta \omega \sum_{\omega_m \in \Omega} a_m(f) e^{2\pi i q(\omega_m)t} q'(\omega_m).$$

Here, $\Delta \omega$ is the distance between two consecutive points ω_{m+1} and ω_m in the partition. The formula is thus a Riemann sum of the integral $\int_{\Omega} \hat{f}(\omega) e^{2\pi i q(\omega)t} q'(\omega) d\omega$. In view of (2.10), this is clearly a discrete representation of the ITDT defined in §2.2. Its usage allows for modeling the desired solution of (2.1) with correct evolution in time.

Theorem 2.6. *Let $\Delta t = T/N$ and $v = (v_1, \dots, v_K)$ be a solution of (2.13) computed at times $t_n = n\Delta t$ for $0 \leq n < N$. Define $u_i(t, x) = \mathcal{I}_{\text{disc}}(v_i(\cdot, x))(t)$ and $f_i(t, x) = \mathcal{I}_{\text{disc}}(g_i(\cdot, x))(t)$. Then $u = (u_1, \dots, u_K)$ solves (2.1) for $0 < t < T$.*

Proof. In the proof we let x be fixed and suppress it from the notation. If f is a function sampled on S and D is given by (2.4) with $j = 1$, then a simple calculation shows that

$$(2.18) \quad a_m(Df) = a_m(f) \sum_j c_{1,j} e^{2\pi i j \omega_m \Delta t}.$$

The second factor on the right is identified as $2\pi i q(\omega_m)$, with q given by (2.6). We record the fact that if v_i solves (2.13) then $a_m(P_i v) = a_m(g_i)$, which in view of (2.18) means that

$$(2.19) \quad (2\pi i q(\omega_m))^{n_i} a_m(v_i) + \sum_{j=0}^{n_i-1} \sum_{k=1}^K L_{ijk} (2\pi i q(\omega_m))^j a_m(v_k) = a_m(g_i).$$

Next, inserting the definition of

$$u_i(t) = \Delta\omega \sum_{\omega_m \in \Omega} a_m(v_i) e^{2\pi i q(\omega_m)t} q'(\omega_m)$$

into (2.1) and differentiating we get

$$\begin{aligned} \mathcal{P}_i u(t, x) = \Delta\omega \sum_{\omega_m \in \Omega} \left[(2\pi i q(\omega_m))^{n_i} a_m(v_i) + \sum_{j=0}^{n_i-1} \sum_{k=1}^K L_{ijk} (2\pi i q(\omega_m))^j a_m(v_k) \right] \\ \times e^{2\pi i q(\omega_m)t} q'(\omega_m). \end{aligned}$$

In view of (2.19) we conclude that

$$\mathcal{P}_i u(t, x) = \Delta\omega \sum_{\omega_m \in \Omega} a_m(g_i) e^{2\pi i q(\omega_m)t} q'(\omega_m) = \mathcal{I}_{\text{disc}}(g_i)(t).$$

By definition, the right-hand side is equal to $f_i(t)$, which completes the proof. \square

Having verified that $\mathcal{I}_{\text{disc}}(v_i)(t)$ evolves correctly in time, we now discuss how the transform $\mathcal{I}_{\text{disc}}$ acts on arbitrary vectors in a discrete setting. Given a solution v_i to (2.13) with known values $v_i(t_n, x)$ at times $t_n = n\Delta t$, $0 \leq n < T/\Delta t$, we first construct the function $\mathcal{I}_{\text{disc}}(v_i(\cdot, x))(t)$ as above. To obtain a function sampled on S we simply evaluate $\mathcal{I}_{\text{disc}}(v_i(\cdot, x))(t)$ at the points $t = k\Delta t$, $k = 0, \dots, N-1$. This immediately generalizes to an arbitrary vector of length N : given any vector (f_0, \dots, f_{N-1}) we define its inverse time dispersion transform by

$$(2.20) \quad (\mathcal{I}_{\text{disc}}(f_n))_k = \Delta\omega \sum_{\omega_m \in \Omega} \left(\Delta t \sum_{n=0}^{N-1} e^{-2\pi i n \omega_m \Delta t} f_n \right) e^{2\pi i q(\omega_m)k\Delta t} q'(\omega_m),$$

for $k = 0, \dots, N-1$.

We now describe how to compute the FTDT (of, e.g., the right-hand side of (2.1)) using discrete sums. For any function f sampled on S we define a modified version of the samples $a_m(f)$ by

$$(2.21) \quad b_m(f) = \Delta t \sum_{n=0}^{N-1} f(n\Delta t) e^{-2\pi i n q(\omega_m) \Delta t},$$

where the frequencies ω_m are as above. Thus $b_m(f)$ is defined by replacing ω_m by $q(\omega_m)$ in the definition of $a_m(f)$. Next, define a function of the continuous variable $t \in [0, T]$ via

$$\mathcal{T}_{\text{disc}}(f)(t) = \Delta\omega \sum_{\omega_m \in \Omega} b_m(f) e^{2\pi i \omega_m t},$$

which in view of the previous discussion is a Riemann sum of the integral defining $\mathcal{T}(f)(t)$. To obtain a function sampled on S we evaluate $\mathcal{T}_{\text{disc}}(f)(t)$ at the points $t = k\Delta t$, $k = 0, \dots, N-1$. Finally, to define the FTDT of a vector we identify $f(n\Delta t)$, $n = 0, \dots, N-1$, with a vector $f = (f_0, \dots, f_{N-1})$ and define the forward time dispersion transform of (f_n) as

$$(\mathcal{T}_{\text{disc}}(f_n))_k = \mathcal{T}_{\text{disc}}(f)(k\Delta t), \quad k = 0, \dots, N-1.$$

As with the inverse time dispersion transform, this immediately generalizes to an arbitrary vector of length N . Given any vector (f_0, \dots, f_{N-1}) we thus define its

forward time dispersion transform by

$$(2.22) \quad (\mathcal{T}_{\text{disc}}(f_n))_k = \Delta\omega \sum_{\omega_m \in \Omega} \left(\Delta t \sum_{n=0}^{N-1} e^{-2\pi i n q(\omega_m) \Delta t} f_n \right) e^{2\pi i \omega_m k \Delta t}.$$

Combined with Theorem 2.6, the previous discussion yields the main result of this section.

Theorem 2.7. *Let $\Delta t = T/N$. Given a source function f_i^{orig} of (2.1), set $g_i = \mathcal{T}_{\text{disc}}(f_i^{\text{orig}})$ and let $v = (v_1, \dots, v_K)$ be a solution of (2.13) computed at times $t_n = n\Delta t$ for $0 \leq n < N$. Define $u_i(t, x) = \mathcal{I}_{\text{disc}}(v_i(\cdot, x))(t)$. Then, for $0 < t < T$, $u = (u_1, \dots, u_K)$ solves (2.1) with f_i^{orig} replaced by $\mathcal{I}_{\text{disc}}(\mathcal{T}_{\text{disc}}(f_i^{\text{orig}}(\cdot, x)))(t)$.*

We stress that, as mentioned in §2.2, the composition of the FTDT and ITDT is not the identity mapping since $\mathcal{I}(\mathcal{T}(f))$ is a bandlimited version of f with frequency support contained in $q(\Omega)$. In particular, suppose we want to simulate a solution to (2.1) with source term f_i^{orig} . To do so, the method prescribed by Theorem 2.7 is to compute $g_i = \mathcal{T}_{\text{disc}}(f_i^{\text{orig}})$, i.e., the (discrete) FTDT of the source term, and solve the discretized equation (2.13) with source term g_i . If v_i is the obtained solution, the theorem implies that $u_i = \mathcal{I}_{\text{disc}}(v_i)$ simulates the evolution of the solution to the original equation (2.1) but with source term

$$f_i = \mathcal{I}_{\text{disc}}(g_i) = \mathcal{I}_{\text{disc}}(\mathcal{T}_{\text{disc}}(f_i^{\text{orig}}))$$

which is an approximation of the bandlimited version of f_i^{orig} with frequency support contained in $q(\Omega)$. Since $q(\Omega) \rightarrow \mathbb{R}$ as $\Delta t \rightarrow 0$, one can make sure to capture the most relevant features of the frequency content of f_i^{orig} by choosing Δt sufficiently small. This is investigated in detail in Section 3 below (see Figure 3).

Remark. Note that a priori, the vector (f_n) in (2.20) and (2.22) should be a vector representing a function sampled on S . If not, interpreting the continuous FTDT and ITDT as Riemann sums lead to different discrete formulas since the range of the index n changes. Note also that although the evolution equation (2.1) is translation invariant, the FTDT and ITDT transforms are not. In particular, we have

$$\mathcal{T}(f)(t) \neq \mathcal{T}(f(\cdot - t_0))(t + t_0), \quad \mathcal{I}(f)(t) \neq \mathcal{I}(f(\cdot - t_0))(t + t_0)$$

in general. However, this is not a problem since we do in fact have

$$\mathcal{I}(\mathcal{T}(f))(t) = \mathcal{I}(\mathcal{T}(f(\cdot - t_0)))(t + t_0)$$

as a consequence of (2.12) (in analogy with the Fourier inversion formula). Thus, when solving a Cauchy problem on, say, $[t_0, T + t_0]$, one can still apply (2.20) and (2.22) to a vector representing a function sampled on $[t_0, T + t_0]$. Heuristically, this amounts to the same as translating the original equation to $[0, T]$, applying the transforms there, and translating back. In view of the discussion preceding this remark one is then simulating a solution to an evolution equation with source term

$$f_i(t) = \mathcal{I}_{\text{disc}}(\mathcal{T}_{\text{disc}}(f_i^{\text{orig}}(\cdot - t_0)))(t + t_0) = \mathcal{I}_{\text{disc}}(\mathcal{T}_{\text{disc}}(f_i^{\text{orig}}))(t).$$

2.4. Fast implementation. In practice, the formulas (2.20) and (2.22) can often be simplified once a specific choice of phase shift function q is made. Specifically,

- using the normalized variable $\omega\Delta t$ can allow the formulas to be interpreted as discrete Fourier transforms which can be implemented using the FFT, and

- using symmetry properties of q and Ω can allow for more efficient algorithms.

Both situations are showcased in the following example.

Example 2.8. Let D be the central difference operator from Example 2.1,

$$Dv(t) = \frac{v(t + \Delta t) - v(t - \Delta t)}{2\Delta t}.$$

Then $q(\omega) = \sin(2\pi\omega\Delta t)/2\pi\Delta t$. Assume as above that $\Delta t = T/N$ where N is the number of sampling points in the time domain, and T is the desired lifespan of the solution. Then $\Omega = \{\omega : |\omega| \leq 1/4\Delta t\}$. To avoid cumbersome notation we will assume that N is even so that $N/2$ is an integer. Inspecting (2.20) we see that we can compute the inner sum by means of the discrete Fourier transform by choosing ω_m appropriately. We pick

$$\omega_m = \frac{1}{4\Delta t} \frac{2m}{N}$$

so that $\omega_m \in \Omega$ when $m = -N/2, \dots, N/2$. Substitution into (2.20) gives after cancellations that

$$(2.23) \quad (\mathcal{I}_{\text{disc}}(f_n))_k = \frac{1}{2N} \sum_{m=-N/2}^{N/2} \left(\sum_{n=0}^{N-1} e^{-2\pi i n m / 2N} f_n \right) e^{i k \sin(\pi m / N)} \cos(\pi m / N).$$

As stated, the inner sum is the value at m of the discrete Fourier transform of \tilde{f} , where \tilde{f} is $f = (f_n)$ zeropadded to twice the length (i.e., the m :th Fourier mode of the vector $(f_0, \dots, f_{N-1}, 0, \dots, 0)$ of length $2N$), and can be computed, e.g., using the FFT. The outer sum is the value at k of a modified discrete inverse Fourier transform (truncated to use only the Fourier modes for $-N/2 \leq m \leq N/2$ instead of the full range $-N \leq m \leq N-1$). If discrete transforms of numerous samples are to be computed, it is advantageous to interpret (2.23) as a linear map acting on the vector (f_n) and compute the corresponding matrix. The cost of this operation scales as $O(N^2 + N \log N)$. Details for implementation in MATLAB can be found in Appendix C.1.

In a similar manner we find by substituting the expression for ω_m into (2.22) that

$$(2.24) \quad (\mathcal{T}_{\text{disc}}(f_n))_k = \frac{1}{2N} \sum_{m=-N/2}^{N/2} \left(\sum_{n=0}^{N-1} e^{-i n \sin(\pi m / N)} f_n \right) e^{2\pi i m k / 2N}.$$

Here, the inner sum is a modified discrete Fourier transform while the outer sum is a truncated discrete inverse Fourier transform at k . The outer sum can be computed using the inverse FFT. We also observe that if $f = (f_n)_{n=0}^{N-1}$ is a vector with real entries, then the inner sum in $(\mathcal{T}_{\text{disc}}(f_n))_k$ equals $b_m(f)/\Delta t$ in the notation above, where $b_{-m}(f) = \overline{b_m(f)}$ and bar denotes complex conjugation. This is a consequence of the fact that sine is an odd function. Similarly, $a_{-m}(f) = \overline{a_m(f)}$, and these symmetries can be used for a more efficient implementation. See Appendix C for details. Note that both (2.23) and (2.24) only contain frequency content up to a quarter of the sampling rate, i.e., up to *half* the Nyquist (folding) frequency. This situation is avoided when a leapfrog scheme can be employed, see Appendix C.2.

Remark. An alternative definition of $\mathcal{I}_{\text{disc}}$ found in the literature [13] is obtained by using Riemann sums to approximate (2.9) instead of (2.10). One such example is

$$(\mathcal{I}_{\text{disc}}^{\text{alt}}(f_n))_k = \Delta\xi \sum_{\xi_m \in q(\Omega)} \left(\Delta t \sum_{n=0}^{N-1} e^{-2\pi i n q^{-1}(\xi_m) \Delta t} f_n \right) e^{2\pi i \xi_m k \Delta t},$$

where the ξ_m are points evenly distributed in $q(\Omega)$ and the first factor is the distance between consecutive points ξ_{m+1} and ξ_m . For implementation using the discrete Fourier transform, a natural option is to choose ξ_m so that $e^{2\pi i \xi_m k \Delta t} = e^{2\pi i m k / 2N}$ for those m for which $\xi_m \in q(\Omega)$. Then $\xi_m = \omega_m$ for m in a subset of $[-N, N-1]$, and the formula above reduces to

$$(\mathcal{I}_{\text{disc}}^{\text{alt}}(f_n))_k = \frac{1}{2N} \sum_{\xi_m \in q(\Omega)} \left(\sum_{n=0}^{N-1} e^{-2\pi i n q^{-1}(\xi_m) \Delta t} f_n \right) e^{2\pi i m k / 2N}.$$

(The absence of the factor q' found in (2.20) is explained by the relation

$$\Delta\xi = \xi_{m+1} - \xi_m = q(\tilde{\omega}_{m+1}) - q(\tilde{\omega}_m) \approx q'(\tilde{\omega}_m)(\tilde{\omega}_{m+1} - \tilde{\omega}_m) = q'(\tilde{\omega}_m)\Delta\tilde{\omega},$$

where $\tilde{\omega}_m$ is the preimage of $\xi_m \in q(\Omega)$.) It is easy to see that with q as in Example 2.8 this results in

$$(\mathcal{I}_{\text{disc}}^{\text{alt}}(f_n))_k = \frac{1}{2N} \sum_{|m| \leq M} \left(\sum_{n=0}^{N-1} e^{-i n \arcsin(\pi m / N)} f_n \right) e^{2\pi i m k / 2N},$$

where M is the largest integer such that $M \leq N/\pi$. Here, the inner sum is a modified discrete Fourier transform while the outer sum can be computed using the inverse FFT.

3. NUMERICAL SIMULATIONS OF A MODEL EQUATION

Here we propose to examine the accuracy of the method by solving a family of ordinary differential equations with known analytic solutions and comparing the resulting numerical solutions, corrected to account for dispersion, with simulations of the analytic expressions. To describe the limitation due to restricting the frequency support inherent in the method, we shall perform tests with source terms of varying frequency support. We consider the simple model

$$(3.1) \quad \begin{cases} u'(t) + u(t) = f(t), \\ u(t) \equiv 0, \quad t < 0, \end{cases}$$

where the source f is a modulated Gaussian window function given by

$$(3.2) \quad f(t) = \frac{1}{\sqrt{2\pi\sigma^2}} \exp\left(-\frac{(t-\mu)^2}{2\sigma^2}\right) \times \exp(2\pi i a(t-\mu)).$$

This is the probability density function of a normal distribution with mean μ and variance σ^2 , modulated by the factor $\exp(2\pi i a(t-\mu))$ with modulation parameter a controlling the location of the frequency support of f .¹ In most applications that we have in mind, the source term is zero at the start of the experiment, and the

¹In contrast to the wave packets discussed in the remark on page 6 and in Appendix A.1, the parameter a is a priori independent of Δt . In addition, in line with the conventions of probability theory, the factor of normalization has been taken here with respect to the usual L^1 norm instead of the L^2 norm.

energy is assumed to have dissipated by the end of the experiment. For this reason we will center f at (say) $t = 5$ by taking $\mu = 5$, and we will take σ so small that $f(t)$ is (practically) zero for $t \leq 0$. In particular, if H is the Heaviside function then we will not distinguish between the functions $f(t)$ and $H(t)f(t)$ in what follows. Taking Fourier transforms we see that if u is a solution of (3.1) then

$$\hat{u}(\omega) = \frac{1}{2\pi i\omega + 1} \hat{f}(\omega),$$

where we identify the first factor on the right as the Fourier transform of $t \mapsto h(t) = e^{-t}H(t)$. By the Fourier inversion formula it follows that u is given by the convolution

$$(3.3) \quad u(t) = h * f(t) = e^{-t} \int_{-\infty}^t e^s f(s) ds, \quad t > 0.$$

Applying the methodology presented in Section 2 we shall compare a sample of $u(t)$ for $0 \leq t \leq 20$ with a numerically computed solution using the time dispersion transforms. To this end, we consider

$$(3.4) \quad \begin{cases} Dv + v = g, & t > 0, \\ v(0) = 0, \end{cases}$$

where D is the central difference operator (appearing in Example 2.8) given by

$$Dv(t) = \frac{v(t + \Delta t) - v(t - \Delta t)}{2\Delta t},$$

and $g = (g_k)$ is the FTDT of f , i.e.,

$$g_k = (\mathcal{T}_{\text{disc}}(f))_k = \frac{1}{2N} \sum_{m=-N/2}^{N/2} \left(\sum_{n=0}^{N-1} e^{-in \sin(\pi m/N)} f(n\Delta t) \right) e^{2\pi i m k / 2N},$$

compare with (2.24). The sample g is computed using the implementation of the FTDT described in Appendix C.1. After solving (3.4) we finally compute the ITDT of $v = (v_n)$ using formula (2.23), again implemented as described in Appendix C.1. To minimize potential wraparound effects resulting from using the dispersion transforms (inherited from the FFT and the inverse FFT) on a modulated source function, we will solve the difference equation for $0 \leq t \leq 20$ and apply a tapered cosine window, affecting the final sample points when $18 \leq t \leq 20$. For transparency, we include plots obtained both with and without this taper.

3.1. Varying the modulation. In Figure 2a we display the analytic solution $u(t)$ computed using (3.3) and sampled at $t = n\Delta t$ with $\Delta t = 0.02$ s. The source function f was chosen to have mean $\mu = 5$ s, variance $\sigma^2 = 0.1$ and modulation $a = 0$. We furthermore show the numerical approximation of $u(t)$ and its error due to the standard central finite difference scheme and the forward Euler scheme. Finally, we use the time dispersion transform method to compute the solution, and show the difference between $u(t)$ and $\mathcal{I}_{\text{disc}}(v)(t)$ with and without using a taper. The numerical results are computed on a desktop with Intel Xeon CPU E5-1650 v3 @ 3.50 GHz, running MATLAB 2017. It takes 0.083 seconds to compute and apply the FTDT to the source function; 0.00049 seconds for the 1000 time integration steps; and 0.077 seconds to compute and apply the ITDT to the solution vector. The time dispersion transform method outperforms the standard schemes by at

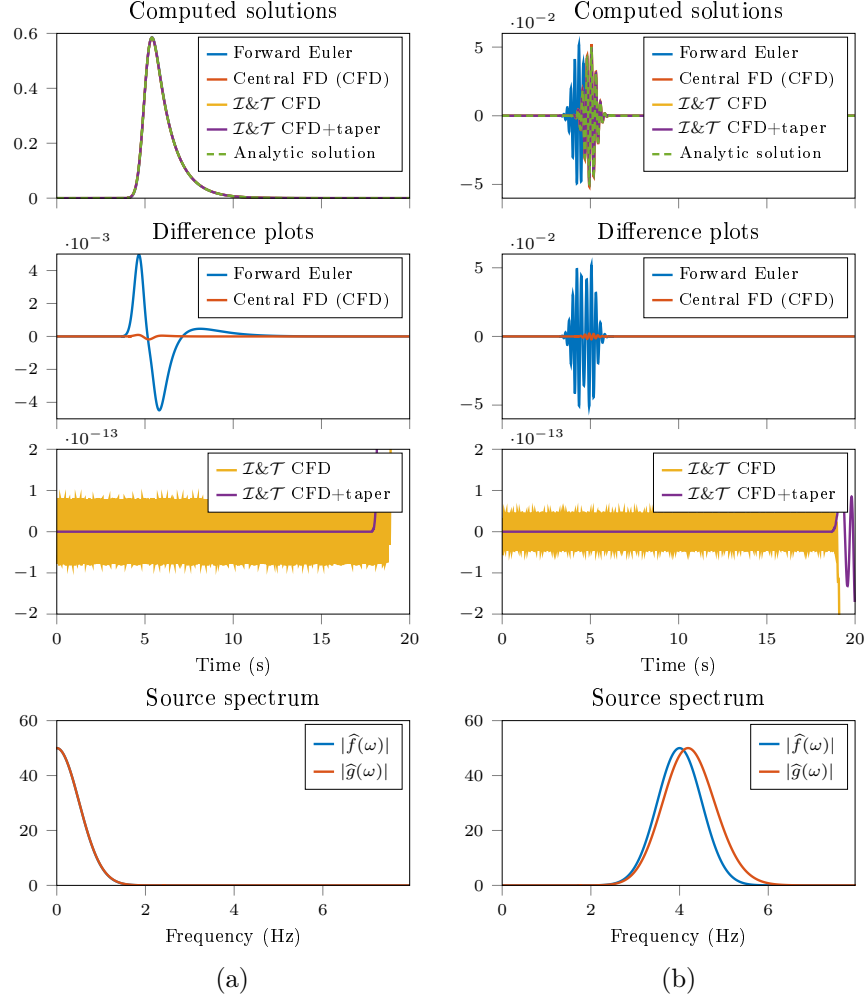


FIGURE 2. Solving (3.1) numerically. The left panels (a) and right panels (b) correspond to an unmodulated and a modulated source, respectively. The difference plots show the difference between the analytic solution and the indicated numerical solutions.

least 9 orders of magnitude – when the taper is used we even obtain accuracy up to an order of 10^{-15} on the range $t \in [0, 18]$.

Figure 2b shows the result of adding a modulation by changing $a = 0$ to $a = 4$. We see that the Fourier support of the source function f still sits comfortably within the critical frequency set $q(\Omega)$, which for $\Delta t = 0.02$ s is given by $q(\Omega) = \{\omega : |\omega| \leq 25/\pi\}$ with ω measured in Hz. The method continues to perform remarkably well, particularly in comparison with the forward Euler and central finite difference schemes. The computation time is identical to the previous case.

3.2. Varying the frequency support. In Figure 3a we have tried to break the method by setting $a = 7.5$. We see that a part of the Fourier support of the source

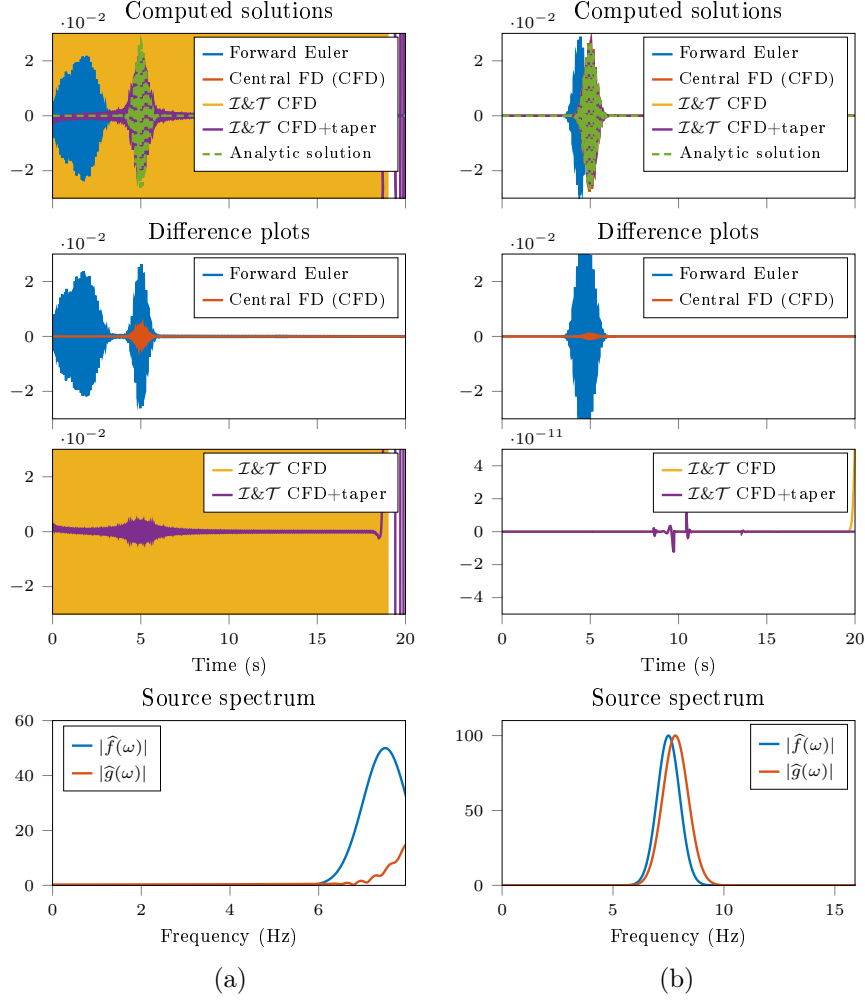


FIGURE 3. Solving (3.1) numerically. The left panels (a) show the effect of a source with too large frequency support for the given spacing Δt . The right panels (b) show the effect of refining the spacing Δt to accommodate.

function f is now outside the critical frequency set $q(\Omega) = \{\omega : |\omega| \leq 25/\pi\}$ and the reconstruction of the analytic solution is quite poor. This is in part due to the strong oscillations of f ; we see in Figure 3a that the Euler scheme also completely breaks down. However, we see that adding a taper results in partial recovery. The computation time is identical to the previous two cases.

As explained in the paragraph following (2.22), we can improve the recovery by decreasing Δt , thus making sure that $q(\Omega)$ is large enough to capture the most relevant frequency content of f . The result of taking $\Delta t = 0.01$ s and keeping all other parameters the same can be seen in Figure 3b. Again, our proposed method performs at least 8 orders of magnitude better than the standard schemes. It takes 0.215 seconds to compute and apply the FDTD to the source function; 0.0175

seconds to compute the 2000 time integration steps; and 0.240 seconds to compute and apply the ITDT to the solution.

4. VISCOELASTIC WAVE SIMULATION

4.1. Memory variables. A common approach to model wave propagation in anelastic media exhibiting both elastic and viscous behavior is to use viscoelastic theory [19]. Assuming that the current value of the stress tensor depends on the history of the strain tensor, the viscoelastic hypothesis is described by the equation for linear viscoelastic rheology,

$$(4.1) \quad \sigma_{ij} = G_{ijkl} * \dot{\varepsilon}_{kl} = \dot{G}_{ijkl} * \varepsilon_{kl},$$

where $\dot{\varepsilon}_{kl}$ is the time derivative of the strain, σ_{ij} is the stress tensor, and G is a fourth order tensor-valued function of time called the elastic tensor (or relaxation function), see [4]. Here $*$ denotes time convolution, and we temporarily employ Einstein notation and sum over repeated indices in this section. The viscoelasticity is often modeled using the notion of a *standard linear solid*, which results in a model of a medium under strain with a mechanical analogy of a spring and dashpot in series, in parallel with another spring (the so-called Maxwell-model description, see [12]). Several standard linear solids can be connected in parallel to emulate a desired viscoelastic behavior.

A popular method to solve (4.1) involves introducing so-called memory variables to handle the convolution operator. Below we recall the resulting equations in two and three dimensions; however our findings also apply to the one-dimensional case, where (4.1) reduces to the visco-acoustic equation $\sigma = G * \dot{\varepsilon}$. For details of the derivation we refer to [19]. We remark that this concerns the case of an isotropic viscoelastic medium. Modeling of wave propagation in anisotropic viscoelastic media has been considered e.g. by Robertsson and Coates [20], and for more on this topic we refer to the mentioned paper and the references therein.

Consider (4.1) in two dimensions ($i, j, k = x, y$) or three dimensions ($i, j, k = x, y, z$). Let π denote the relaxation modulus corresponding to pressure waves analogous to $\lambda + 2\mu$ in the elastic case, where λ and μ are the Lamé parameters. Let $\tau_{\varepsilon n}^p$ and $\tau_{\varepsilon n}^s$ be the stress relaxation times of the n th mechanism for pressure waves and shear waves, respectively. To shorten the expressions, let δ_{ij} denote the Kronecker delta and introduce the tensors

$$(4.2) \quad C_{ijkl} = \frac{1}{N} \sum_{n=1}^N \left[\left(\pi \frac{\tau_{\varepsilon n}^p}{\tau_{\sigma n}} - 2\mu \frac{\tau_{\varepsilon n}^s}{\tau_{\sigma n}} \right) \delta_{ij} \delta_{kl} + \mu \frac{\tau_{\varepsilon n}^s}{\tau_{\sigma n}} (\delta_{ik} \delta_{jl} + \delta_{jk} \delta_{il}) \right],$$

and

$$(4.3) \quad \tilde{C}_{ijkl}^{(n)} = \left(\pi \left(\frac{\tau_{\varepsilon n}^p}{\tau_{\sigma n}} - 1 \right) - 2\mu \left(\frac{\tau_{\varepsilon n}^s}{\tau_{\sigma n}} - 1 \right) \right) \delta_{ij} \delta_{kl} + \mu \left(\frac{\tau_{\varepsilon n}^s}{\tau_{\sigma n}} - 1 \right) (\delta_{ik} \delta_{jl} + \delta_{jk} \delta_{il})$$

for $1 \leq n \leq N$. Wave propagation in a viscoelastic medium with N sets of standard linear solids can then be described by Newton's second law

$$(4.4) \quad \rho \dot{v}_i = \partial_j \sigma_{ij} + f_i$$

together with

$$(4.5) \quad \dot{\sigma}_{ij} = C_{ijkl} \partial_k v_l + \frac{1}{N} \sum_{n=1}^N r_{ijn},$$

where v_i denotes the components of particle velocity, f_i the source terms and ρ is density (assumed to be time independent). Each r_{ijn} is a memory variable satisfying the equation

$$(4.6) \quad \dot{r}_{ijn} = -\frac{1}{\tau_{\sigma n}} \left\{ r_{ijn} + \tilde{C}_{ijk\ell}^{(n)} \partial_k v_\ell \right\}.$$

Observe that (4.4)–(4.6) constitutes a system of equations of the form (2.1). Indeed, considering the three-dimensional (3D) case, denote v_x, v_y, v_z by u_1, u_2, u_3 , denote the six distinct σ_{ij} , $i, j = x, y, z$, by u_4, \dots, u_9 , and the $6N$ distinct memory variables r_{ijn} by u_{10}, \dots, u_{6N+9} . Inspecting the equations above we see that the spatial operators involved are linear and independent of t . Hence, the results of Section 2 (in particular Theorems 2.5–2.7) are applicable to this case. Equations (4.4)–(4.6) are then discretized in time by

$$(4.7) \quad \rho DV_i = \partial_j \Sigma_{ij} + g_i,$$

$$(4.8) \quad D\Sigma_{ij} = C_{ijk\ell} \partial_k V_\ell + \frac{1}{N} \sum_{n=1}^N R_{ijn},$$

$$(4.9) \quad DR_{ijn} = -\frac{1}{\tau_{\sigma n}} \left\{ R_{ijn} + \tilde{C}_{ijk\ell}^{(n)} \partial_k V_\ell \right\},$$

for some choice of finite difference operator D .

4.2. Model introduction. We apply the theory of the previous section on a viscoelastic wave modeling example, using the leapfrog scheme described in detail in Appendix B to solve (4.7)–(4.9). Since leapfrog schemes are the simplest energy-conserving integrators [8] this is a natural choice in order to avoid numerical dissipation errors and thus isolate the effects caused by numerical dispersion errors.

We use the open-source 2D modeling engine SOFI2D developed by Bohlen *et al.* [3] to perform the 2D viscoelastic simulation. Time is discretized into steps of constant length Δt . Similarly, continuous space is discretized into a 2D grid with spacing of Δx and Δz in the x and z directions. The wave equation is then solved using staggering of quantities in space, and using the leapfrog method to integrate the wave equation in time [23]. The spatial derivatives are efficiently approximated with a central 1D finite difference stencil of half-order 6:

$$\partial_x f(x_j) \approx \sum_{l=1}^6 \frac{\alpha_l}{\Delta x_j} \left(f(x_j + (l - \frac{1}{2})\Delta x_j) - f(x_j - (l - \frac{1}{2})\Delta x_j) \right),$$

for which the weights are given in Table 1. These weights correspond to an equirip-

TABLE 1. The central finite difference weights used to compute the spatial first-order derivatives, truncated to 4 digits.

α_1	α_2	α_3	α_4	α_5	α_6
1.2508	−0.1203	0.0321	−0.0101	0.0030	−0.0007

ple (minimax) filter that keeps the group-velocity error of the first-order derivative approximation confined to within 0.1%. Such ‘optimal’ finite difference coefficients are customary in geophysical finite difference modeling [18], see e.g. [12] for the

design procedure. We state the Courant-Friedrichs-Lewy (CFL) condition that ensures stability of the 2D simulation given the second-order accurate integration of the equations in time, as a function of the chosen discretizations and maximum velocity encountered in the simulation:

$$v_{\max} \Delta t \sqrt{\left(\sum_{l=1}^6 \left| \frac{\alpha_l}{\Delta x} \right| \right)^2 + \left(\sum_{l=1}^6 \left| \frac{\alpha_l}{\Delta z} \right| \right)^2} \leq 1.$$

We will see that the maximum velocity present in the model is 4700 m/s, and we choose a spatial discretization of $\Delta x = \Delta z = 12.5$ m. The maximum stable time-step then follows as $\Delta t = 1.3$ ms. We choose this as the ‘coarse’ time-step. We can compare this coarse solution against an additional ‘fine’ simulation, which uses a time-step of $\Delta t = 0.013$ ms, which we consider to be the reference solution for our purposes.

The model used for the simulation is the Marmousi 2 model [16], which provides a density model (ρ), a model for compressional wave velocities (v_p) and transverse shear velocities (v_s) which reflect the instantaneous elastic deformation modes for (4.4)–(4.6):

$$\begin{aligned} \pi &= \rho v_p^2, \\ \mu &= \rho v_s^2. \end{aligned}$$

The models for ρ , v_p and v_s are shown in Figure 4a. For the viscoelastic modeling we furthermore create a variable so-called Q model, by smoothing the v_s and v_p models and normalizing them to a maximum Q of 350, as shown in Figure 4b. Here Q is a quality factor that measures the amount of energy dissipation, with $Q \rightarrow \infty$ corresponding to the elastic, undamped case. Additionally shown in the figures are the source location at $(x, z) = (0, 25)$ and a series of recorders along the entire upper model boundary at $(x, z) = (n \cdot 12.5, 62.5)$ for $n = -679, \dots, 679$, with the coordinates in meters. One specific recorder at $(x, z) = (4625, 62.5)$ is highlighted as an arbitrarily shown recorder that will be zoomed in upon in the results.

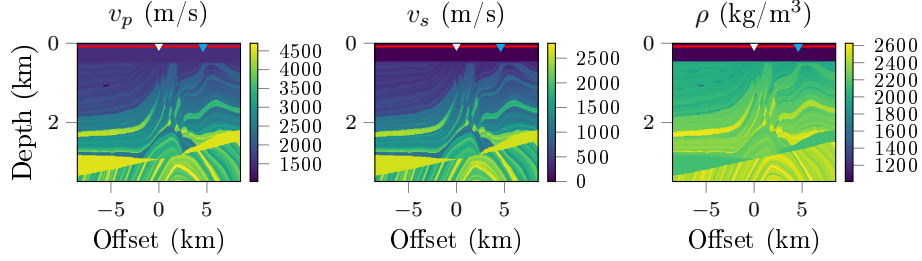
The source-time function of the model is a typical seismic source wavelet, described as a 15 Hz peak frequency Ricker wavelet with a time-delay of 0.15 s:

$$(4.10) \quad f(t) = (1 - 2\pi^2 15^2 (t - 0.15)^2) e^{-\pi^2 15^2 (t - 0.15)^2}.$$

The source is injected as an explosive source that radiates equally in all directions. The recorders along the upper model boundary record the pressure variations (the diagonal stress components $\sigma_{xx} + \sigma_{zz}$) as a function of time at every Δt simulated.

4.3. The elastic model results. We first test the theory in an elastic case, in which we take $Q \rightarrow \infty$ so there is no damping, and with $N = 0$ so there is no relaxation mechanism at all. The evolution of the wave equation is then computed from time 0 to 5 s with three model runs:

- (1) Using a coarse time-step of $\Delta t = 1.3$ ms without correcting the source or receiver time-series,
- (2) Using a coarse time-step of $\Delta t = 1.3$ ms, but using the FTDT to correct the source injection time-series (4.10), and the ITDT to correct the recorded time-series,
- (3) Using a fine time-step of $\Delta t = 0.013$ ms as a reference solution.



(a) The elastic Marmousi model.

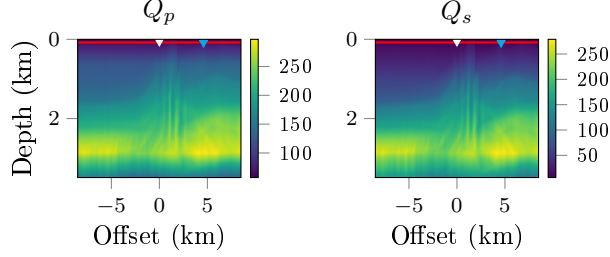
(b) The Q model for the viscoelastic case.

FIGURE 4. The compressional wave velocity (v_p), transverse shear wave velocity (v_s) and density (ρ) of the Marmousi 2 elastic model in (a), and the Q model for the compressional wave (Q_p) and the transverse shear wave (Q_s) in (b). The source location is denoted by a white triangle in the top center of the models, the receiver line is denoted by the red line on the top of the models, a single recording station is denoted in the cyan triangle in the top-right of the models, which is used for the detailed zoom in Figures 5–6.

As the implemented wave equation solver scales linearly in time (keeping the spatial discretization $\Delta x = \Delta z = 12.5$ m in place), the third simulation thus costs 100 times more computational time. In this elastic instance, it takes 50 seconds to compute simulations (1) and (2), but 75 minutes for the simulation (3). Application in simulation (2) of the FDTD on the source-time function takes half a second to compute, and applying the ITDT to *all* 1359 recorded signals takes seven seconds in total. This is, essentially, of negligible cost compared to the fine simulation (3).

After finishing all the computations, we subsample the fine simulation to be able to compare the results sample-by-sample. The computed result is then shown in Figure 5. We show a zoom on a single recording (its location is denoted in cyan in Figure 4 but was chosen arbitrarily). It is clearly visible that the coarse simulation (1) created a recording that differs starkly from that made within the fine simulation (3). Conversely, after applying the time dispersion transforms on the source-time function and the receiver time-function, we obtain a solution that follows the correct phase and amplitude of the fine simulation. The two images below the graph in Figure 5 subtract the results of the coarse simulations from the fine simulation – confirming that the correction procedure in this paper removes the dispersion error effectively for all recordings. The sum of all 1359 root mean square (RMS) errors along all traces is 1634 for the coarse case, and 1.6 for the simulation

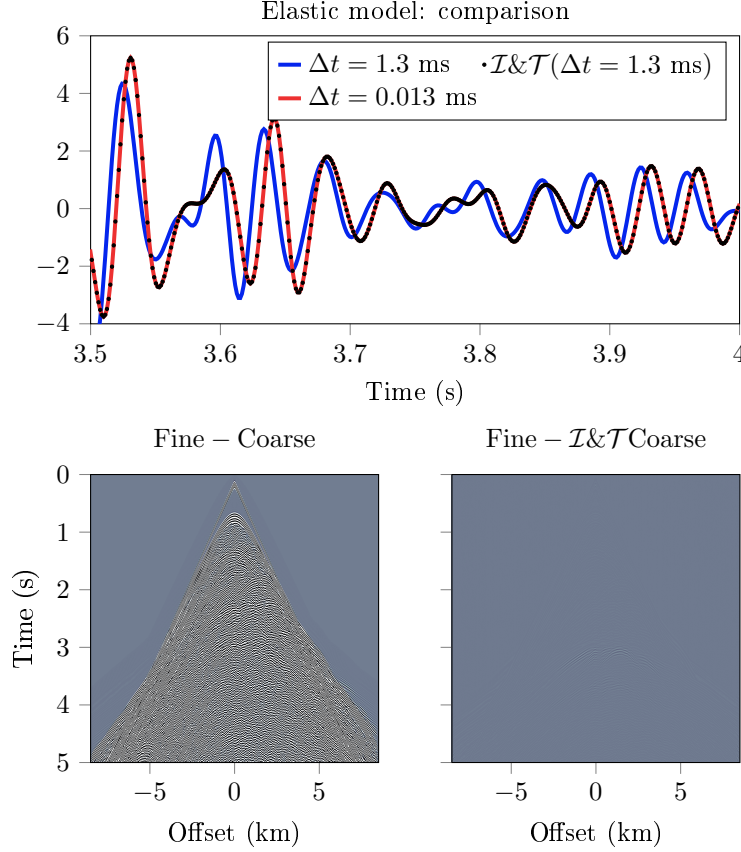


FIGURE 5. Removing dispersion for an elastic case. The top panel zooms in on a single recorder at (4625, 62.5) (a so-called ‘trace’ at offset 4.625 km). The graph in blue represents the coarse time-step solution, the graph in red the reference solution with a fine time-step. The graph in black dots uses the frequency-modification suggested in this paper on the source and recording of another coarse simulation. The bottom two panels show the difference between the three different data sets for all 1359 recordings at varying offset.

with the proposed time dispersion transforms – the error energy is thus reduced by a factor 1018. The remaining errors seem to be of localized impact only, affecting strong peaks and troughs in the time-series, but do not seem to accumulate over time.

4.4. The viscoelastic model results. The viscoelastic model uses three relaxation mechanisms ($N = 3$) to model the spatially heterogeneous Q model. Apart from these changes to the physical model, we proceed in exactly the same way as in the previous example. The computed result is displayed in Figure 6. The amplitudes in this model decrease with time as exemplified by the now 10 times smaller

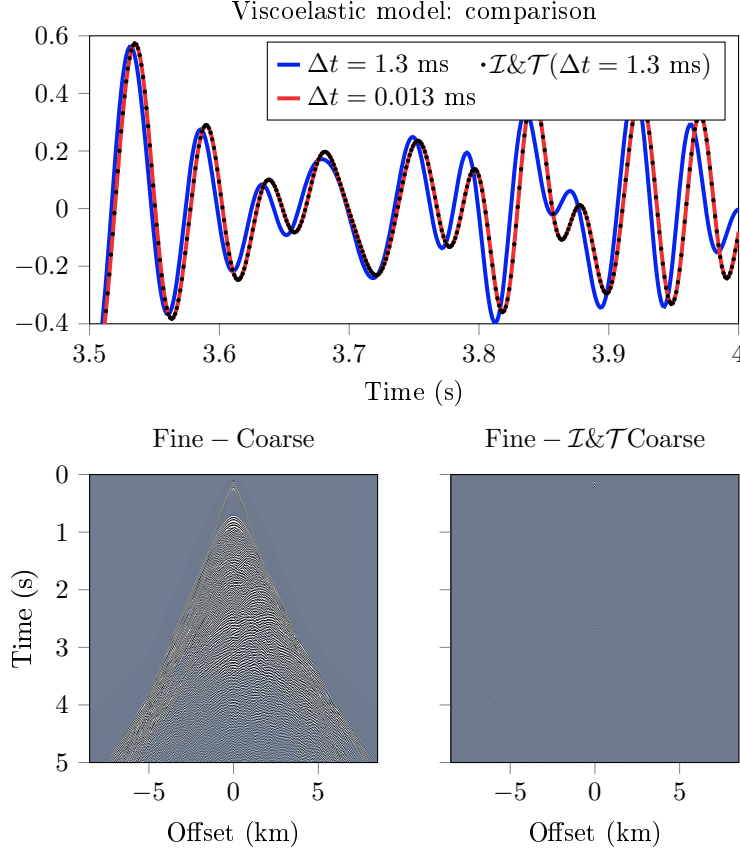


FIGURE 6. Removing dispersion for a viscoelastic case. The top of the figure zooms in on a single recorded trace at offset 4.625 km. The graph in blue represents the coarse time-step solution, the graph in red the reference solution with a fine time-step. The graph in black dots uses the frequency-modification suggested in this paper on the source and recording of another coarse simulation. The bottom two figures show the difference between the three different data sets for all 1359 recordings at varying offset.

amplitudes in the graph compared to the elastic case, due to the damping. Like the elastic case before, the coarse simulation with $\Delta t = 1.3$ ms differs significantly from the fine simulation with $\Delta t = 0.013$ ms. Conversely, applying the proposed corrections to the coarse simulation creates an adequate fit to the fine simulation. The computational time of all simulations is roughly doubled compared to the elastic simulation at 100 seconds for the coarse simulations and over 2 hours for the viscoelastic simulation. The FDTD and ITDT are still applied to the source-time function in half a second and to all 1359 traces in 7 seconds, respectively. The sum of all 1359 RMS errors along all traces is 212 for the coarse case, and 1.47 for the coarse case using the proposed transforms. Again, the error energy is reduced

(now by a factor of 144) at very little additional cost. Again, these errors do not accumulate for longer simulation times.

5. CONCLUSIONS

We have described a method for removing the numerical errors that are caused by approximating the time derivative by a finite difference operator when modeling linear evolution equations. The method is based on integral transforms (realized as certain Fourier integral operators). We have shown that their application results in a correct simulation of the desired evolution for any length of time. For a given initial value problem, the approximation error is governed primarily by the extent to which the source term can be considered to be sufficiently bandlimited, which has been illustrated by numerical examples. We have also demonstrated the performance and accuracy of the method on the simulation of non-dissipative (elastic) and dissipative (viscoelastic) wave simulations.

ACKNOWLEDGEMENTS

The research of Jens Wittsten was supported by the Swedish Research Council Grant 2015-03780. The research of Erik Koene was supported by SNF grant 2-77220-15. We gratefully acknowledge the work of Thomas Bohlen, Denise De Nil, Daniel Köhn and Stefan Jetschny for the open-source code SOFI2D used in the viscoelastic simulations. We also wish to thank Christof Stork for interesting discussions.

APPENDIX A. AUXILIARY RESULTS

A.1. Fourier integral operators. Here we show how the dispersion transforms can be naturally understood as Fourier integral operators (FIO). In this context it will be convenient to view Δt as a small (semiclassical) parameter $h > 0$. We define the semiclassical Fourier transform of a function $f(t)$ by

$$\mathcal{F}_h(f)(\eta) = \frac{1}{\sqrt{h}} \int e^{-2\pi i t \eta / h} f(t) dt,$$

so that $\widehat{f}(\omega) = h^{\frac{1}{2}} \mathcal{F}_h(f)(\omega h)$. The Fourier inversion formula then takes the form

$$f(t) = \frac{1}{\sqrt{h}} \int e^{2\pi i t \eta / h} \mathcal{F}_h(f)(\eta) d\eta.$$

Standard references for semiclassical analysis are Martinez [17] and Zworski [25].

Recall the normalized phase shift function q_0 introduced in (2.7) which satisfies $q_0(\omega h)/h = q(\omega)$, and define Ω_0 by $\eta = \omega h \in \Omega_0$ if and only if $\omega \in \Omega$. By changing variables in (2.10) it is easy to see that

$$(A.1) \quad \mathcal{I}(f)(t) = \frac{1}{\sqrt{h}} \int_{\Omega_0} e^{2\pi i t q_0(\eta)/h} q_0'(\eta) \mathcal{F}_h(f)(\eta) d\eta.$$

Note that $q'(\omega) = q_0'(\omega h)$ and $q^{-1}(\omega) = q_0^{-1}(\omega h)/h$, which implies that $q'(q^{-1}(\omega)) = q_0'(q_0^{-1}(\omega h))$, so making the change of variables $\eta = \omega h$ in (2.8) similarly gives

$$(A.2) \quad \mathcal{T}(f)(t) = \frac{1}{\sqrt{h}} \int_{q_0(\Omega_0)} e^{2\pi i t q_0^{-1}(\eta)/h} \frac{1}{q_0'(q_0^{-1}(\eta))} \mathcal{F}_h(f)(\eta) d\eta.$$

If f is a function whose semiclassical Fourier transform has support contained in a set U we will say that f is h -bandlimited in U . Applying the ITDT to a function

already h -bandlimited in Ω_0 can be naturally understood, in view of (A.1), as the action of a semiclassical FIO (call it A) which in $\mathbb{R} \times \Omega_0 \subset T^*(\mathbb{R})$ has phase function $\varphi(t, \eta) = tq_0(\eta)$ and symbol $a(t, \eta) = q'_0(\eta)$. A is associated to the canonical transformation locally given by

$$\chi : (\varphi'_\eta(t, \eta), \eta) \mapsto (t, \varphi'_t(t, \eta)),$$

i.e., by (2.15). Similarly, \mathcal{T} is a semiclassical FIO (call it B) which in $\mathbb{R} \times q_0(\Omega_0)$ has phase function $\psi(t, \eta) = tq_0^{-1}(\eta)$ and symbol $b(t, \eta) = 1/q'_0(q_0^{-1}(\eta))$. B is associated to the inverse map χ^{-1} . The composition BA acts as the identity operator on functions h -bandlimited in Ω_0 . The composition AB acts as the identity operator on functions h -bandlimited in $q_0(\Omega_0)$. Furthermore, using the Fourier inversion formula and arguments similar to those in the proof of Theorem 2.5, it is straightforward to check that $B\mathcal{P}_i = \mathcal{P}_iB$, so that, as operators acting on functions h -bandlimited in Ω_0 , $\mathcal{P}_i = B\mathcal{P}_iA$.

Note that the previous discussion can also be had in the framework of microlocal analysis for fixed Δt , i.e., without viewing Δt as a semiclassical parameter. Our choice was made in preparation for §A.1.1 below. If one instead takes the other viewpoint and repeats the arguments above one finds that the dispersion transforms are realized as FIOs associated to the canonical map

$$\chi_q : (tq'(\omega), \omega) \mapsto (t, q(\omega))$$

and its inverse. This gives a formula for the appropriate discrete operator to be used for given choice of discrete approximation D of the time derivative, even in the case when time-dependent coefficients are allowed in (2.1). In fact, if q is the corresponding phase shift function, then the previous paragraph shows that \mathcal{P}_i should be replaced by (a discretized version of)

$$Q_i = \mathcal{T}\mathcal{P}_i\mathcal{I}.$$

By Egorov's theorem, this operator is a *pseudodifferential operator* with an integral representation

$$Q_iv(t) = \int_{\Omega} e^{2\pi it\omega} Q_i(t, \omega) \hat{v}(\omega) d\omega,$$

where, with abuse of notation, the symbol $Q_i(t, \omega)$ is a function defined on phase space (omitting all dependence on the spatial variable x). Assuming that $\mathcal{P}_i = p_{in_i}(t)\partial_t^{n_i}$ plus lower order terms, the principal symbol $\sigma(Q_i)$ of Q_i is given by

$$\sigma(\mathcal{P}_i)(\chi_q(t, \omega)) = p_{in_i}(t/q'(\omega))(2\pi iq(\omega))^{n_i}.$$

The lower order terms of Q_i can be expressed in terms of χ_q and derivatives of the symbol of \mathcal{P}_i . However, due to the dependence of ω for example in $p_{in_i}(t/q'(\omega))$, the two factors on the right cannot be separated in such a way that the operator $\mathcal{T}\mathcal{P}_i\mathcal{I}$ is directly realized as a finite difference operator. Investigating the case of time-dependent coefficients is therefore beyond the scope of the current paper and will not be pursued further here.

A.1.1. Dynamics of wave packets. For $(x_0, \xi_0) \in T^*(\mathbb{R})$, a function of the form

$$\varphi_{(x_0, \xi_0)}(t) = (2/h)^{\frac{1}{4}} e^{2\pi i(t-x_0)\xi_0/h} e^{-\pi(t-x_0)^2/h}$$

will be called a *Gaussian wave packet*. Here $\varphi_{(x_0, \xi_0)}$ has been normalized with respect to the usual inner product in $L^2(\mathbb{R})$. We see that when $h \ll 1$, $\varphi_{(x_0, \xi_0)}(t) =$

$O(h^\infty)$ is negligible if $t \neq x_0$, where $O(h^\infty)$ means $O(h^N)$ for all $N > 0$. Similarly,

$$(A.3) \quad \mathcal{F}_h(\varphi_{(x_0, \xi_0)})(\eta) = (2/h)^{\frac{1}{4}} e^{-2\pi i x_0 \eta/h} e^{-\pi(\eta - \xi_0)^2/h}$$

is negligible if $\eta \neq \xi_0$. These notions are combined in the following.

Definition A.1. Let $u = u(h)$, $0 < h \leq h_0$, be a family of functions in $L^2(\mathbb{R})$. We say that u is *microlocally small* near $(x_0, \xi_0) \in T^*(\mathbb{R})$ if the inner product

$$|(u, \varphi_{(x, \xi)})_{L^2(\mathbb{R})}| = \left| \int_{\mathbb{R}} u(t) e^{-2\pi i(t-x)\xi/h} e^{-\pi(t-x)^2/h} dt \right| = O(h^\infty)$$

uniformly for (x, ξ) in a neighborhood of (x_0, ξ_0) . The complement of such points (x_0, ξ_0) is called the *semiclassical wavefront set* of u , denoted $\text{WF}_h(u)$.

Another common name for the semiclassical wavefront set is *frequency set*, usually denoted $\text{FS}(u)$. For other equivalent definitions, including those employing the *Fourier-Bros-Iagolnitzer* (FBI) transform we refer to Martinez [17] and Zworski [25]. Our presentation is inspired by Faure [6].

As alluded to above, $\text{WF}_h(\varphi_{(x_0, \xi_0)}) = \{(x_0, \xi_0)\}$ which is made evident by computing the inner product

$$(\varphi_{(x_0, \xi_0)}, \varphi_{(x, \xi)})_{L^2(\mathbb{R})} = e^{-2\pi i(x_0 - x)(\xi_0 + \xi)/2h} e^{-\pi(x_0 - x)^2/2h} e^{-\pi(\xi_0 - \xi)^2/2h}.$$

The following result describes how the wavefront set of a Gaussian wave packet is affected by the dispersion transforms.

Proposition A.2. Let $\varphi_{(x_0, \xi_0)}$ be a Gaussian wave packet, and let χ be the canonical map given by (2.15). Then

$$\text{WF}_h(\mathcal{I}(\varphi_{(x_0, \xi_0)})) = \{\chi(x_0, \xi_0)\} = \{(x_0/q'_0(\xi_0), q_0(\xi_0))\},$$

$$\text{WF}_h(\mathcal{T}(\varphi_{(x_0, \xi_0)})) = \{\chi^{-1}(x_0, \xi_0)\} = \{(x_0 q'_0(q_0^{-1}(\xi_0)), q_0^{-1}(\xi_0))\}.$$

Proof. We will prove the first identity, the proof of the second being similar is left to the reader. Changing variables in (A.1) we see that

$$\mathcal{I}(\varphi_{(x_0, \xi_0)}) = \mathcal{F}_h^{-1}(\mathbf{1}_{q_0(\Omega_0)} \mathcal{F}_h(\varphi_{(x_0, \xi_0)})(q_0^{-1}(\cdot))),$$

so an application of the Plancharel formula gives

$$\begin{aligned} (\mathcal{I}(\varphi_{(x_0, \xi_0)}), \varphi_{(x, \xi)})_{L^2(\mathbb{R})} &= (\mathcal{F}_h(\mathcal{I}(\varphi_{(x_0, \xi_0)})), \mathcal{F}_h(\varphi_{(x, \xi)}))_{L^2(\mathbb{R})} \\ &= (\mathbf{1}_{q_0(\Omega_0)} \mathcal{F}_h(\varphi_{(x_0, \xi_0)})(q_0^{-1}(\cdot)), \mathcal{F}_h(\varphi_{(x, \xi)}))_{L^2(\mathbb{R})}. \end{aligned}$$

In view of (A.3), $(\mathcal{I}(\varphi_{(x_0, \xi_0)}), \varphi_{(x, \xi)})_{L^2(\mathbb{R})}$ is therefore equal to the integral

$$\int_{q_0(\Omega_0)} e^{-2\pi i x_0 q_0^{-1}(\eta)/h} e^{-\pi(q_0^{-1}(\eta) - \xi_0)^2/h} e^{2\pi i x \eta/h} e^{-\pi(\eta - \xi)^2/h} d\eta.$$

Due to the quadratic terms in the exponential, this is clearly $O(h^\infty)$ in the semiclassical limit $h \rightarrow 0$ if and only if there are no η_0 such that $\eta_0 - \xi = q_0^{-1}(\eta_0) - \xi_0 = 0$, i.e., such that $\xi = \eta_0 = q_0(\xi_0)$. Writing the remaining oscillatory factors as $e^{2\pi i \phi(\eta)/h}$ with $\phi(\eta) = x\eta - x_0 q_0^{-1}(\eta)$, it follows from the principle of non-stationary phase that the integral is also $O(h^\infty)$ unless $\phi'(\eta_0) = 0$, see e.g., [25, Lemma 3.10]. But $\phi'(\eta_0) = 0$ implies that

$$y = \frac{x_0}{q'_0(q_0^{-1}(\eta_0))} = \frac{x_0}{q'_0(\xi_0)},$$

so $\text{WF}_h(\mathcal{I}(\varphi_{(x_0, \xi_0)})) \subset \{(x_0/q'_0(\xi_0), q_0(\xi_0))\}$. That we in fact have equality follows from the discussion above together with the method of stationary phase. We refer

to Hörmander [11, Section 7.7] for a discussion of both non-degenerate ($\phi''(\eta_0) \neq 0$) as well as degenerate ($\phi''(\eta_0) = 0$) critical points. \square

A.2. Initial conditions. Let u_i be the solution to (2.1) with initial conditions (2.2). Note that by the Fourier inversion formula

$$(A.4) \quad \phi_{ij}(x) = \partial_t^j u_i(0, x) = \int_{-\infty}^{\infty} (2\pi i \omega)^j \hat{u}_i(\omega, x) d\omega.$$

By virtue of Theorem 2.5, $\mathcal{T}(u_i)$ solves the corresponding FD equation modified to account for time dispersion, namely (2.13). Since the initial condition is time-independent, it cannot be modified using the time dispersion transform, so the natural choice is to impose the same initial conditions for (2.13) as for (2.1). However, letting v_i be the solution to (2.13) with initial conditions (2.2), so that $\partial_t^j v_i(0, x) = \phi_{ij}(x)$, this introduces an approximation error between $\mathcal{T}(u_i)$ and v_i . Indeed, by the Fourier inversion formula and the definition of $\mathcal{T}(u_i)$ we have

$$\partial_t^j \mathcal{T}(u_i)(0, x) = \int_{\Omega} (2\pi i \omega)^j \hat{u}_i(q(\omega), x) d\omega$$

which does not equal ϕ_{ij} in view of (A.4). If we set

$$(A.5) \quad \psi_{ij}(x) = \int_{\Omega} (2\pi i \omega)^j \hat{u}_i(q(\omega), x) d\omega,$$

we see that the “correct” FD initial value problem to solve in order to obtain a sampling of $\mathcal{T}(u_i)$ would be (2.13) with initial condition $\partial_t^j v_i(0, x) = \psi_{ij}(x)$, but since ψ_{ij} is defined using knowledge of u_i this is not possible in practice. On the other hand, since $\mathcal{T}(u_i)$ and v_i have the same evolution in time according to Theorem 2.5, $\mathcal{T}(u_i)$ will continue to stay close to v_i for all t as long as ψ_{ij} is a good approximation of ϕ_{ij} . The accuracy of approximation is ensured by the following lemma. To keep the presentation general, we make the assumptions that

- $\mathbf{1}_{\Omega}(\omega)$ converges pointwise to 1 as $\Delta t \rightarrow 0$, i.e., $\Omega \subset \mathbb{R}$ exhausts \mathbb{R} in the limit as $\Delta t \rightarrow 0$,
- $q(\omega)$ converges pointwise to ω as $\Delta t \rightarrow 0$,
- $|q(\omega)| \geq c|\omega|$ for $\omega \in \Omega$ where c is a real-valued constant independent of Δt .

We also assume that Ω has a decomposition $\Omega = \Omega_{\text{inn}} \cup \Omega_{\text{out}}$ consisting of an inner and outer region where $\Omega_{\text{inn}} \rightarrow \mathbb{R}$ as $\Delta t \rightarrow 0$, such that for some real-valued constants C_1, C_2, C_3 independent of Δt ,

- $q'(\omega) \geq C_1$ if $\omega \in \Omega_{\text{inn}}$,
- $|\omega| \geq C_2/\Delta t$ if $\omega \in \Omega_{\text{out}}$,
- Ω_{out} has Lebesgue measure $|\Omega_{\text{out}}| \leq C_3/\Delta t$.

To illustrate, if $q(\omega)$ is the function described in Example 2.1 then these assumptions are satisfied with $c = 2/\pi$, $\Omega_{\text{inn}} = \{\omega : |\omega| \leq (8\Delta t)^{-1}\}$ and $C_1 = 1/\sqrt{2}$, $C_2 = 1/8$, $C_3 = 1/4$.

Lemma A.3. *Let u_i solve (2.1)–(2.2) and let ψ_{ij} be given by (A.5). Then*

$$\lim_{\Delta t \rightarrow 0} \psi_{ij}(x) = \phi_{ij}(x), \quad 0 \leq j \leq n_i - 1,$$

and the convergence is uniform with respect to $x \in X$ in the sense of (2.3). The rate of convergence depends on the discretization (2.4) of the time derivative.

Proof. Inspecting the definitions and recalling that $\Omega = \Omega_{\text{inn}} \cup \Omega_{\text{out}}$ we see that the result is proved by showing

$$(A.6) \quad \lim_{\Delta t \rightarrow 0} \left(\int_{\Omega_{\text{inn}}} + \int_{\Omega_{\text{out}}} \right) (2\pi i \omega)^j \widehat{u}_i(q(\omega), x) d\omega = \int_{-\infty}^{\infty} (2\pi i \omega)^j \widehat{u}_i(\omega, x) d\omega,$$

which is essentially a consequence of the Lebesgue dominated convergence theorem. For the benefit of the reader we include the details.

Before treating each integral on the left separately we make two observations. Firstly, (2.3) implies

$$(A.7) \quad \int_{-\infty}^{\infty} (1 + |\omega|^2)^k |\widehat{u}_i(\omega, x)|^2 d\omega < \infty, \quad 0 \leq k \leq n_i,$$

which means that $|\widehat{u}_i(\omega, x)| \leq g_i(\omega, x)^{1/2} (1 + |\omega|^2)^{-n_i/2}$ for some integrable function $\omega \mapsto g_i(\omega, x)$, where $g_i(\omega, x) \rightarrow 0$ as $|\omega| \rightarrow \infty$ by the Riemann-Lebesgue lemma. Secondly, by assumption we have $|q(\omega)| \geq c|\omega|$ for $\omega \in \Omega$ with c independent of Δt , so

$$(A.8) \quad \int_{\Omega} |(2\pi i \omega)^j \widehat{u}_i(q(\omega), x)| d\omega \leq \left(\frac{2\pi}{c} \right)^j \int_{\Omega} |q(\omega)|^j |\widehat{u}_i(q(\omega), x)| d\omega.$$

We begin by treating the first integral on the left of (A.6). Recall that by our standing assumptions, $u_i(t, x)$ is integrable in t which means that $\widehat{u}_i(\omega, x)$ is continuous in ω , while $\mathbf{1}_{\Omega_{\text{inn}}}(\omega) \rightarrow 1$ and $q(\omega) \rightarrow \omega$ pointwise as $\Delta t \rightarrow 0$. Next, note that

$$\int_{\Omega_{\text{inn}}} |q(\omega)|^j |\widehat{u}_i(q(\omega), x)| d\omega = \int_{q(\Omega_{\text{inn}})} \frac{|\xi|^j |\widehat{u}_i(\xi, x)|}{q'(q^{-1}(\xi))} d\xi \leq \frac{1}{C_1} \int_{-\infty}^{\infty} |\xi|^j |\widehat{u}_i(\xi, x)| d\xi$$

since $\xi \in q(\Omega_{\text{inn}})$ implies that $\omega = q^{-1}(\xi) \in \Omega_{\text{inn}}$ for which we have $q'(\omega) \geq C_1$ by assumption. Since C_1 is independent of Δt and the right-most integral is convergent by (A.7), Lebesgue's dominated convergence theorem together with (A.8) implies that

$$\lim_{\Delta t \rightarrow 0} \int_{\Omega_{\text{inn}}} (2\pi i \omega)^j \widehat{u}_i(q(\omega), x) d\omega = \int_{-\infty}^{\infty} (2\pi i \omega)^j \widehat{u}_i(\omega, x) d\omega.$$

To treat the second integral on the left of (A.6), note that

$$|q(\omega)|^j |\widehat{u}_i(q(\omega), x)| \leq \frac{|q(\omega)|^j}{(1 + |q(\omega)|^2)^{(n_i-1)/2}} \frac{g_i(\omega, x)^{1/2}}{(1 + |q(\omega)|^2)^{1/2}} \leq \frac{g_i(\omega, x)^{1/2}}{(1 + c^2 \omega^2)^{1/2}}$$

for $0 \leq j \leq n_i - 1$. Since $|\omega| \geq C_1/\Delta t$ when $\omega \in \Omega_{\text{out}}$ and $|\Omega_{\text{out}}| \leq C_2/\Delta t$, it is then easy to see that

$$\int_{\Omega_{\text{out}}} |q(\omega)|^j |\widehat{u}_i(q(\omega), x)| d\omega \leq \frac{C_2}{C_1 c} \sup_{\omega \in \Omega_{\text{out}}} g_i(\omega, x)^{1/2}$$

with g_i and c independent of Δt . Since $g_i(\omega, x) \rightarrow 0$ as $|\omega| \rightarrow \infty$ it follows that the supremum above tends to 0 as $\Delta t \rightarrow 0$. In view of (A.8) we conclude that

$$\lim_{\Delta t \rightarrow 0} \int_{\Omega_{\text{out}}} (2\pi i \omega)^j \widehat{u}_i(q(\omega), x) d\omega = 0.$$

This proves (A.6). From the proof it is clear that the convergence is uniform with respect to $x \in X$ in the sense of (2.3), and that the rate of convergence depends on $q(\omega)$. Since the definition of q is equivalent to the choice of discretization (2.4) of the time derivative, the last statement of the lemma follows. \square

A.3. Non-matching finite difference schemes. Here we briefly discuss what can happen if non-matching FD approximations are used to define D^j in (2.4). To highlight the effect we choose a simple prototype of the evolution equation (2.1): Let $u = (u_1, u_2)$ and consider the system

$$(A.9) \quad \partial_t u_1(t, x) = L_{11}u_1(t, x) + L_{12}u_2(t, x),$$

$$(A.10) \quad \partial_t u_2(t, x) = L_{21}u_1(t, x) - Cu_2(t, x),$$

where the L_{ij} are linear spatial operators independent of t and C is a constant. An example of such a system is provided by the usage of memory variables in (4.8)–(4.9). We will as before let D denote a scheme satisfying all prior assumptions and use it to model the time derivative in (A.9), but we assume that (A.10) is an auxiliary equation and allow a different scheme to model its time derivative. (This can be desirable e.g. in large-scale supercomputer global seismological simulations where the stress and displacement are updated at every step in time, but the memory variables only every 4 steps in time, which saves computational costs without being dramatically worse in performance.) Denote it by

$$\tilde{D}v_i(t, x) = \sum_n \tilde{c}_{1,n} v_i(t + n\Delta t, x),$$

and define

$$\tilde{q}(\omega) = \frac{1}{2\pi i} \sum_n \tilde{c}_{1,n} e^{2\pi i \omega \Delta t n}.$$

The next result explains how the discretized equations should be modified in order to accurately model the evolution of a solution to (A.9)–(A.10).

Proposition A.4. *Let $u = (u_1, u_2)$ be a solution of (A.9)–(A.10). Set*

$$G(t) = \int_{\Omega} \frac{2\pi i \tilde{q}(\omega) + C}{2\pi i q(\omega) + C} e^{2\pi i t \omega} d\omega,$$

and define $v_i = \mathcal{T}(u_i)$ for $i = 1, 2$. Then $v = (v_1, v_2)$ solves

$$(A.11) \quad Dv_1(t, x) = L_{11}v_1(t, x) + L_{12}v_2(t, x),$$

$$(A.12) \quad \tilde{D}v_2(t, x) = L_{21}v_1(\cdot, x) * G(t) - Cv_2(t, x),$$

for each value of t , where $$ denotes time convolution.*

Proof. Note that G is well defined since q is real-valued and the integration domain is a compact set. Also,

$$(A.13) \quad \hat{G}(\omega) = \mathbf{1}_{\Omega}(\omega) \frac{2\pi i \tilde{q}(\omega) + C}{2\pi i q(\omega) + C}.$$

Fix x and suppress it from the notation, and let L_j be the 1×2 system $L_j = (L_{j1}, L_{j2})$, $j = 1, 2$. Using the Fourier inversion formula and the definition of v_1 we have

$$Dv_1(t) - L_1v(t) = \int_{\Omega} [(2\pi i q(\omega) - L_{11})\hat{u}_1(q(\omega)) - L_{12}\hat{u}_2(q(\omega))] e^{2\pi i t \omega} d\omega.$$

Taking a Fourier transform of (A.9) and evaluating at $q(\omega)$ shows that

$$[(2\pi i q(\omega) - L_{11})\hat{u}_1(q(\omega)) - L_{12}\hat{u}_2(q(\omega))] = 0,$$

so v_1 solves (A.11).

To prove that v_2 solves (A.12), we observe that

$$(A.14) \quad \hat{u}_2(q(\omega)) = \frac{1}{2\pi i q(\omega) + C} L_{21} \hat{u}_1(q(\omega)).$$

This formula is easily obtained by taking a Fourier transform of (A.10), solving for \hat{u}_2 and evaluating the result at $q(\omega)$. It follows that

$$\tilde{D}v_2(t) + Cv_2(t) = \int_{-\infty}^{\infty} (2\pi i \tilde{q}(\omega) + C) \hat{v}_2(\omega) e^{2\pi i t \omega} d\omega.$$

Since $\hat{v}_2(\omega) = \mathbf{1}_{\Omega}(\omega) \hat{u}_2(q(\omega))$ we find in view of (A.13) and (A.14) that

$$\tilde{D}v_2(t) + Cv_2(t) = \int_{-\infty}^{\infty} \hat{G}(\omega) L_{21} \hat{u}_1(q(\omega)) \mathbf{1}_{\Omega}(\omega) e^{2\pi i t \omega} d\omega.$$

Since $\hat{u}_1(q(\omega)) \mathbf{1}_{\Omega}(\omega) = \hat{v}_1(\omega)$, this is equivalent to (A.12) by virtue of the Fourier inversion formula. \square

Proposition A.4 shows that the price one has to pay for using different FD schemes to approximate the time derivatives in (A.9) and in (A.10), is the appearance of a convolution in (A.12). Ignoring the convolution results in an approximation of the desired evolution that can be estimated in terms of the amount by which (A.13) differs from 1.

Note that if the constant C in (A.12) is replaced by a spatial operator L_{22} which, while independent of t , is not simply constant in x then the previous result has to be modified accordingly. By minor changes, the proof of Proposition A.4 shows that the result remains valid if G is replaced by

$$G(t) = \int_{\Omega} \frac{\tilde{q}(\omega)}{q(\omega)} e^{2\pi i t \omega} d\omega,$$

and (A.12) is replaced by

$$\tilde{D}v_2(t, x) = (L_{21}v_1(\cdot, x) + L_{22}v_2(\cdot, x)) * G(t).$$

We remark that G is well defined due to the assumption that $|q(\omega)| \geq c|\omega|$ for $\omega \in \Omega$.

APPENDIX B. VISCOELASTIC FINITE DIFFERENCE EQUATIONS

Here we discuss the removal of time dispersion from 2D and 3D viscoelastic FD modeling for a specific leapfrog scheme developed in [19] (see Bohlen [2] for an explicit implementation). Recall (4.4)–(4.6). The time derivative of a function is approximated by

$$(B.1) \quad Df(t, x) = \frac{f(t + \frac{1}{2}\Delta t) - f(t - \frac{1}{2}\Delta t)}{\Delta t}.$$

In this case, the phase shift function $q(\omega)$ is found to be

$$(B.2) \quad q(\omega) = \frac{\sin(\pi\omega\Delta t)}{\pi\Delta t},$$

which is invertible for $\omega \in \Omega$ where $\Omega = [-\frac{1}{2\Delta t}, \frac{1}{2\Delta t}]$. Here the upper limit $1/2\Delta t$ coincides with the Nyquist frequency which is an improvement compared to finite difference scheme employed in Section 3. The drawback is the need to use a time average of the memory variables as described below.

Let $\mathbf{M}f(t, x)$ denote the time average

$$(B.3) \quad \mathbf{M}f(t, x) = \frac{1}{2}(f(t + \frac{1}{2}\Delta t, x) + f(t - \frac{1}{2}\Delta t, x))$$

of a function $f(t, x)$. Equations (4.4)–(4.6) are discretized in time by

$$(B.4) \quad \rho \mathbf{D}V_i = \partial_j \Sigma_{ij} + g_i,$$

$$(B.5) \quad \mathbf{D}\Sigma_{ij} = C_{ijkl} \partial_k V_\ell + \frac{1}{N} \sum_{n=1}^N \mathbf{M}R_{ijn},$$

$$(B.6) \quad \mathbf{D}R_{ijn} = -\frac{1}{\tau_{\sigma n}} \left\{ \mathbf{M}R_{ijn} + \tilde{C}_{ijkl}^{(n)} \partial_k V_\ell \right\},$$

where C_{ijkl} and $\tilde{C}_{ijkl}^{(n)}$ are given by (4.2)–(4.3). If in addition the spatial derivatives are discretized using a fourth-order staggered forward operator and backward operator as is done by Bohlen [2], one arrives at the discrete equations [2, (A.3)–(A.17)] after some straightforward calculations. (In this paper we have extended it to a twelfth-order scheme.) We then have the following.

Theorem B.1. *Let v_i and σ_{ij} solve (4.4)–(4.5), with memory variables solving (4.6). Define $V_i = \mathcal{T}(v_i)$, $\Sigma_{ij} = \mathcal{T}(\sigma_{ij})$ and $g_i = \mathcal{T}(f_i)$. Then for each value of t , V_i and Σ_{ij} solve (B.4) exactly and (B.5) approximately, where the R_{ijn} are exact solutions to (B.6). In the numerical simulations of Section 4, the approximation error is $O(\Delta t^2)$.*

Before the proof we recall from §4.1 that, according to Theorem 2.5, the functions V_i , Σ_{ij} and R_{ijn} are exact solutions to the equations obtained by removing all occurrences of the averaging operator \mathbf{M} from (B.4)–(B.6).

Proof. We will keep x fixed and omit it from the notation. We first observe that for a function $f(t)$ we have

$$(B.7) \quad \widehat{\mathbf{M}f}(\omega) = \hat{f}(\omega) \cos(\pi\omega\Delta t).$$

We also record the fact that if v_i and σ_{ij} solve (4.4)–(4.6) then

$$(B.8) \quad \rho(2\pi i\omega)\hat{v}_i(\omega) = \partial_j \hat{\sigma}_{ij}(\omega) + \hat{f}_i(\omega),$$

$$(B.9) \quad (2\pi i\omega)\hat{\sigma}_{ij}(\omega) = C_{ijkl} \partial_k \hat{v}_\ell(\omega) + \frac{1}{N} \sum_{n=1}^N \hat{r}_{ijn}(\omega),$$

where

$$(B.10) \quad \hat{r}_{ijn}(\omega) = -\frac{\tilde{C}_{ijkl}^{(n)} \partial_k \hat{v}_\ell(\omega)}{1 + 2\pi i\omega\tau_{\sigma n}}, \quad 1 \leq n \leq N,$$

which follows from (4.6) and a straightforward computation.

By definition, $\hat{V}_i(\omega) = \mathbf{1}_\Omega(\omega)\hat{v}_i(q(\omega))$. Similar formulas hold for Σ_{ij} and g_i . Hence,

$$\rho \mathbf{D}V_i(t) - \partial_j \Sigma_{ij}(t) = \int_{\Omega} [\rho(2\pi i q(\omega))\hat{v}_i(q(\omega)) - \partial_j \hat{\sigma}_{ij}(q(\omega))] e^{2\pi i t \omega} d\omega$$

by the Fourier inversion formula. Using (B.8) evaluated at $q(\omega)$ instead of ω we see that the right-hand side is equal to $\int_{\Omega} \hat{f}_i(q(\omega)) e^{2\pi i t \omega} d\omega = g_i(t)$, which proves that (B.4) holds.

Next, write

$$D\Sigma_{ij}(t) - C_{ijk\ell}\partial_k V_\ell(t) = \int_{\Omega} [2\pi i q(\omega)\widehat{\sigma}_{ij}(q(\omega)) - C_{ijk\ell}\partial_k \widehat{v}_\ell(q(\omega))] e^{2\pi i t\omega} d\omega.$$

Applying (B.9) evaluated at $q(\omega)$ instead of ω we get

$$(B.11) \quad D\Sigma_{ij}(t) - C_{ijk\ell}\partial_k V_\ell(t) = \int_{\Omega} \left(\frac{1}{N} \sum_{n=1}^N \widehat{r}_{ijn}(q(\omega)) \right) e^{2\pi i t\omega} d\omega.$$

We now take a Fourier transform in t of (B.6). Using (B.7), elementary computations show that

$$\widehat{R}_{ijn}(\omega) = -\frac{\widetilde{C}_{ijk\ell}^{(n)}\partial_k \widehat{V}_\ell(\omega)}{\cos(\pi\omega\Delta t) + 2\pi i q(\omega)\tau_{\sigma n}} = \widehat{r}_{ijn}(q(\omega)) \frac{1 + 2\pi i q(\omega)\tau_{\sigma n}}{\cos(\pi\omega\Delta t) + 2\pi i q(\omega)\tau_{\sigma n}}$$

for $\omega \in \Omega$, where the last identity follows by inserting the definition of V_i and inspecting (B.10). Using (B.7) again it is straightforward to check that

$$\widehat{r}_{ijn}(q(\omega)) = \widehat{MR}_{ijn}(\omega) + \widehat{R}_{ijn}(\omega)(1 - \cos(\pi\omega\Delta t)) \frac{2i \sin(\pi\omega\Delta t)\tau_{\sigma n}}{\Delta t + 2i \sin(\pi\omega\Delta t)\tau_{\sigma n}}.$$

where the last factor is uniformly bounded for $\omega \in \Omega$, and the second factor is $O(\Delta t^2)$ when ω is restricted to a bounded, Δt -independent set. In the simulations in Section 4 it turns out that $\widehat{R}_{ijn}(\omega)$ is indeed supported in a Δt -independent set, see Figure 7. In view of (B.11) we thus conclude that

$$D\Sigma_{ij}(t) - C_{ijk\ell}\partial_k V_\ell(t) = \int_{\Omega} \left(\frac{1}{N} \sum_{\ell=1}^N \widehat{MR}_{ijn}(\omega) \right) e^{2\pi i t\omega} d\omega + O(\Delta t^2).$$

The result now follows by applying the Fourier inversion formula to the integral on the right. \square

Naturally, there are also versions of Theorems 2.6 and 2.7 corresponding to Theorem B.1. We leave for the reader to fill in the details.

APPENDIX C. IMPLEMENTATION

Here we show how to implement the discrete dispersion transforms in MATLAB in two specific cases, namely the finite difference scheme from Example 2.8 that is used in the numerical simulations of Section 3, and the leapfrog scheme from Appendix B that is used in the viscoelastic simulations of Section 4. The interested reader should then be able to adapt the procedure to other cases without difficulty.

C.1. Central difference scheme. Consider the finite difference operator from Example 2.8 and recall (2.23). We see by inspection that we can view $(\mathcal{I}_{\text{disc}}(f_n))_k$ in matrix terms as row $k+1$ of a matrix A applied to $\tilde{f} = (f_0, \dots, f_{N-1}, 0, \dots, 0)$, where $A = (a_{(k+1)(n+1)})_{k,n=0}^{2N-1}$ is the matrix with element

$$a_{(k+1)(n+1)} = \frac{1}{2N} \sum_{m=-N/2}^{N/2} e^{-2\pi i n m / 2N} e^{i k \sin(\pi m / N)} \cos(\pi m / N)$$

at position $(k+1)(n+1)$. We may view the sum as ranging over $-N \leq m \leq N-1$ with terms for $-N/2+1 \leq |m| \leq N$ being zero; in particular the term for $m = -N$ is zero, and so would the term with $m = N$ be. Changing variables $m \mapsto -m$ we

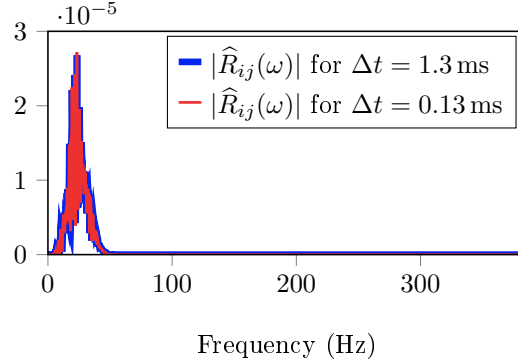


FIGURE 7. The spectrum of the summed, dispersed memory variables $R_{ij} = \sum_n R_{ijn}$ as recorded at $(z, x) = (262.5, 62.5)$ in the viscoelastic simulations from Section 4. Note how the energy fits well within the Nyquist frequency $1/(2 \cdot 0.0013) = 385$ Hz, even for the coarsest possible time-step $\Delta t = 1.3$ ms. Moreover, the energy remains limited to about 40 Hz, also for simulations with a smaller $\Delta t = 0.13$ ms.

thus see that this is the inverse discrete Fourier transform of $m \mapsto g_k(m)$ evaluated at n , where

$$g_k(m) = \begin{cases} e^{-ik \sin(\pi m/N)} \cos(\pi m/N) & \text{for } |m| \leq N/2, \\ 0 & \text{otherwise.} \end{cases}$$

A can therefore be computed by applying the inverse FFT to the matrix with columns g_{k+1} and taking real transpose, e.g., via

```
function [A] = finite_difference_ITDT(N)
A1 = exp( -1i * sin([0:N/2]*pi/(N))' * [0:2*N-1] );
A = ifft( cos([0:N/2]'*pi/N) .* A1, 2*N, 'symmetric' );
A = A(1:N,1:N);
end
```

where we also take advantage of conjugate symmetry. The last line truncates the matrix so it can be applied directly to the original vector f without having to zeropad the sample manually as this is already built in.

Similarly, by inspecting (2.24) we see that we can view $(\mathcal{T}_{\text{disc}}(f_n))_k$ as row $k+1$ of a matrix B applied to $\tilde{f} = (f_0, \dots, f_{N-1}, 0, \dots, 0)$, where $B = (b_{(k+1)(n+1)})_{k,n=0}^{2N-1}$ is the matrix with element

$$b_{(k+1)(n+1)} = \frac{1}{2N} \sum_{m=-N/2}^{N/2} e^{-in \sin(\pi m/N)} e^{2\pi i m k / 2N}$$

at position $(k+1)(n+1)$. As before we may view the sum as ranging over $-N \leq m \leq N-1$ with terms for $-N/2+1 \leq |m| \leq N$ being zero. We thus see that this is the inverse discrete Fourier transform of $m \mapsto h_n(m)$ evaluated at k , where

$$h_n(m) = \begin{cases} e^{-in \sin(\pi m/N)} & \text{for } |m| \leq N/2, \\ 0 & \text{otherwise.} \end{cases}$$

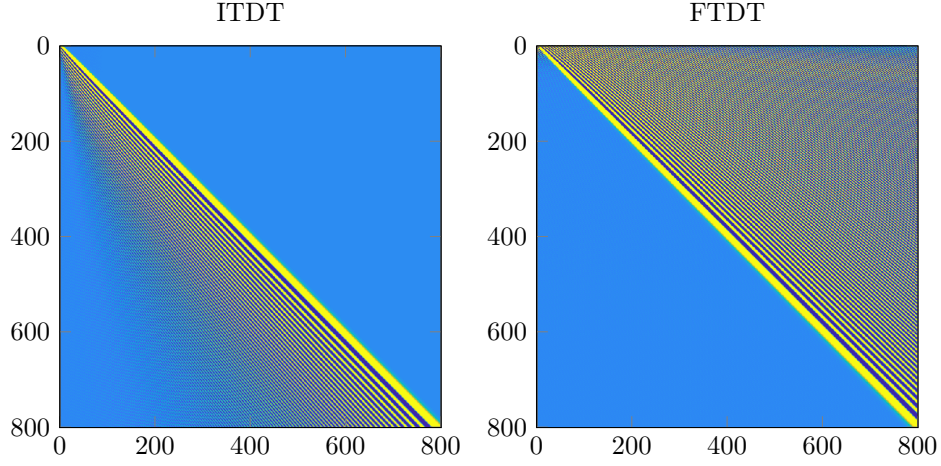


FIGURE 8. Visual illustration of matrix representations of the inverse time dispersion transform (left) and the forward time dispersion transform (right).

B can therefore be computed (without taking transpose) by applying the inverse FFT to the matrix with columns h_{n+1} , e.g., via

```
function [B] = finite_difference_FTDT(N)
B1 = exp( -1i * sin([0:N/2]*pi/N)' * [0:2*N-1] );
B = ifft( B1, 2*N, 'symmetric' );
B = B(1:N,1:N);
end
```

As before, the last line truncates the matrix thus avoiding the need to zeropad the sample f manually. The matrices A and B are depicted in Figure 8.

C.2. Leapfrog scheme. Consider now the leapfrog scheme from Appendix B and recall that in this case, the phase shift function is $q(\omega) = \sin(\pi\omega\Delta t)/\pi\Delta t$ by (B.2), so q is invertible for $\omega \in \Omega$ where $\Omega = [-\frac{1}{2\Delta t}, \frac{1}{2\Delta t}]$. We remark that this is not the same as replacing Δt by $\Delta t/2$ in the previous subsection since the time-step size for each individual function is in fact Δt . Repeating the arguments in Example 2.8 for this choice of q we find by inserting

$$\omega_m = \frac{1}{2\Delta t} \frac{m}{N}, \quad m = -N+1, \dots, N,$$

into (2.20) that

$$(\mathcal{I}_{\text{disc}}(f_n))_k = \frac{1}{2N} \sum_{m=-N+1}^N \left(\sum_{n=0}^{N-1} e^{-2\pi i n m / 2N} f_n \right) e^{2ik \sin(\pi m / 2N)} \cos(\pi m / 2N).$$

Here the inner sum is the value at m of the discrete Fourier transform of the vector (f_0, \dots, f_{N-1}) zeropadded to twice the length. The outer sum is the value at k of a modified discrete inverse Fourier transform (without truncation). This is the image of f under the action of row $k+1$ of the matrix $A = (a_{(k+1)(n+1)})_{k,n=0}^{2N-1}$ with

element

$$a_{(k+1)(n+1)} = \frac{1}{2N} \sum_{m=-N+1}^N e^{-2\pi i n m / 2N} e^{2ik \sin(\pi m / 2N)} \cos(\pi m / 2N)$$

at position $(k+1)(n+1)$. Changing variables $m \mapsto -m$ we identify this as the inverse discrete Fourier transform of $m \mapsto g_k(m)$ evaluated at n , where

$$g_k(m) = e^{-2ik \sin(\pi m / 2N)} \cos(\pi m / 2N) \quad \text{for } m = -N, \dots, N-1.$$

A can be computed by applying the inverse FFT to the matrix with columns g_{k+1} and taking real transpose via

```
function [A] = leapfrog_ITDT(N)
A1 = exp( -2i * sin([0:N-1]*pi/(2*N))' * [0:2*N-1] );
A = ifft( cos([0:N-1]*pi/(2*N)) .* A1, 2*N, 'symmetric' );
A = A(1:N,1:N);
end
```

Next, by inserting the expression for ω_m (shifted one index) into (2.22) we find that

$$(\mathcal{T}_{\text{disc}}(f_n))_k = \frac{1}{2N} \sum_{m=-N}^{N-1} \left(\sum_{n=0}^{N-1} e^{-2in \sin(\pi m / 2N)} f_n \right) e^{2\pi i m k / 2N}.$$

Thus we can view $(\mathcal{T}_{\text{disc}}(f_n))_k$ as row $k+1$ of a matrix B applied to (f_0, \dots, f_{N-1}) zeropadded to twice the length, where $B = (b_{(k+1)(n+1)})_{k,n=0}^{2N-1}$ has element

$$b_{(k+1)(n+1)} = \frac{1}{2N} \sum_{m=-N}^{N-1} e^{-2in \sin(\pi m / 2N)} e^{2\pi i m k / 2N}$$

at position $(k+1)(n+1)$. This is the inverse discrete Fourier transform of $m \mapsto h_n(m)$ evaluated at k , where

$$h_n(m) = e^{-2in \sin(\pi m / 2N)} \quad \text{for } m = -N, \dots, N-1.$$

B can be computed by applying the inverse FFT to the matrix with columns h_{n+1} via

```
function [B] = leapfrog_FTDT(N)
B1 = exp( -2i * sin([0:N-1]*pi/(2*N))' * [0:2*N-1] );
B = ifft( B1, 2*N, 'symmetric' );
B = B(1:N,1:N);
end
```

REFERENCES

1. D.A. Anderson, J.C. Tannehill, and R.H. Pletcher, *Computational fluid mechanics and heat transfer*, McGraw-Hill, 1984.
2. Thomas Bohlen, *Parallel 3-d viscoelastic finite difference seismic modelling*, Computers & Geosciences **28** (2002), no. 8, 887–899.
3. Thomas Bohlen, Denise De Nil, Daniel Köhn, and Stefan Jetschny, *Sofi2d seismic modeling with finite differences: 2d – elastic and viscoelastic version*, Karlsruhe Institute of Technology, 2016.
4. Richard M. Christensen, *Theory of viscoelasticity: an introduction*, second ed., Academic Press, 1982.
5. Lawrence C. Evans, *Partial differential equations*, second ed., Graduate texts in Mathematics, vol. 19, American Mathematical Society, 2010.

6. Frédéric Faure, *Semiclassical origin of the spectral gap for transfer operators of a partially expanding map*, Nonlinearity **24** (2011), no. 5, 1473–1498.
7. Bengt Fornberg, *A practical guide to pseudospectral methods*, vol. 1, Cambridge university press, 1998.
8. Ernst Hairer, Christian Lubich, and Gerhard Wanner, *Geometric numerical integration: structure-preserving algorithms for ordinary differential equations*, vol. 31, Springer Science & Business Media, 2006.
9. Klaus A Hoffmann and Steve T Chiang, *Computational fluid dynamics volume i*, Engineering Education System, 2000.
10. Olav Holberg, *Computational aspects of the choice of operator and sampling interval for numerical differentiation in large-scale simulation of wave phenomena*, Geophysical prospecting **35** (1987), no. 6, 629–655.
11. Lars Hörmander, *The analysis of linear partial differential equations I–IV*, Springer Verlag, 1983–1985.
12. M Kindelan, A Kamel, and P Sguazzero, *On the construction and efficiency of staggered numerical differentiators for the wave equation*, Geophysics **55** (1990), no. 1, 107–110.
13. Erik FM Koene, Johan OA Robertsson, Filippo Broggin, and Fredrik Andersson, *Eliminating time dispersion from seismic wave modeling*, Geophysical Journal International **213** (2018), no. 1, 169–180.
14. Peter D Lax and Robert D Richtmyer, *Survey of the stability of linear finite difference equations*, Communications on pure and applied mathematics **9** (1956), no. 2, 267–293.
15. Randall J LeVeque, *Finite difference methods for ordinary and partial differential equations: steady-state and time-dependent problems*, vol. 98, Siam, 2007.
16. Gary S Martin, Kurt J Marfurt, and Shawn Larsen, *Marmousi-2: An updated model for the investigation of avo in structurally complex areas*, SEG Technical Program Expanded Abstracts 2002, Society of Exploration Geophysicists, 2002, pp. 1979–1982.
17. André Martinez, *An introduction to semiclassical and microlocal analysis*, Springer, 2002.
18. Peter Moczo, Johan O A Robertsson, and Leo Eisner, *The finite-difference time-domain method for modeling of seismic wave propagation*, Advances in Geophysics **48** (2007), 421–516.
19. Johan O A Robertsson, Joakim O Blanch, and William W Symes, *Viscoelastic finite-difference modeling*, Geophysics **59** (1994), no. 9, 1444–1456.
20. Johan OA Robertsson and Richard T Coates, *Finite-difference modeling of Q for qP- and qS-waves in anisotropic media*, SEG Technical Program Expanded Abstracts 1997, Society of Exploration Geophysicists, 1997, pp. 1846–1849.
21. Christof Stork, *Eliminating nearly all dispersion error from fd modeling and rtm with minimal cost increase*, 75th EAGE Conference & Exhibition incorporating SPE EUROPEC 2013, 2013.
22. Vladimir A Titarev and Eleuterio F Toro, *Ader: Arbitrary high order godunov approach*, Journal of Scientific Computing **17** (2002), no. 1-4, 609–618.
23. Jean Virieux, *P-sv wave propagation in heterogeneous media: Velocity-stress finite-difference method*, Geophysics **51** (1986), no. 4, 889–901.
24. Meixia Wang and Sheng Xu, *Finite-difference time dispersion transforms for wave propagation*, Geophysics **80** (2015), no. 6, WD19–WD25.
25. Maciej Zworski, *Semiclassical analysis*, vol. 138, American Mathematical Soc., 2012.

(Jens Wittsten) CENTRE FOR MATHEMATICAL SCIENCES, LUND UNIVERSITY, SWEDEN AND
DEPARTMENT OF ENGINEERING, UNIVERSITY OF BORÅS, SWEDEN
E-mail address: jensw@maths.lth.se

(Erik F. M. Koene) INSTITUTE OF GEOPHYSICS, ETH-ZÜRICH, SWITZERLAND
E-mail address: erik.koene@erdw.ethz.ch

(Fredrik Andersson) INSTITUTE OF GEOPHYSICS, ETH-ZÜRICH, SWITZERLAND
E-mail address: fredrik.andersson@erdw.ethz.ch

(Johan O. A. Robertsson) INSTITUTE OF GEOPHYSICS, ETH-ZÜRICH, SWITZERLAND
E-mail address: johan.robertsson@erdw.ethz.ch